Uncoordinated Massive Wireless Networks: Spatiotemporal Models and Multiaccess Strategies

Giovanni Chisci, *Member, IEEE*, Hesham ElSawy, *Senior Member, IEEE*, Andrea Conti, *Senior Member, IEEE*, Mohamed-Slim Alouini, *Fellow, IEEE*, and Moe Z. Win, *Fellow, IEEE*

***Abstract*— The massive wireless networks (MWNs) enable surging applications for the Internet of Things and cyber physical systems. In these applications, nodes typically exhibit stringent power constraints, limited computing capabilities, and sporadic traffic patterns. This paper develops a spatiotemporal model to characterize and design uncoordinated multiple access (UMA) strategies for MWNs. By combining stochastic geometry and queueing theory, the paper quantifies the scalability of UMA via the maximum spatiotemporal traffic density that can be accommodated in the network, while satisfying the target operational constraints (e.g., stability) for a given percentile of the nodes. The developed framework is then used to design UMA strategies that stabilize the node data buffers and achieve desirable latency, buffer size, and data rate.**

***Index Terms*— Wireless networks, Internet of Things, uncoordinated multiple access, meta distribution of the SINR.**

I. Introduction

MASSIVE WIRELESS NETWORKS (MWNs) enable the communication among many nodes including sensors, actuators, machines, vehicles, drones, and many other smart objects (things), and will significantly contribute to the supply of big data and automation of the foreseen smart world. Realizing such a massive wireless connectivity is an important foundation for the Internet of things (IoT) and cyber physical systems (CPSs) [1], [2]. Such massively many connected nodes are required to communicate with each other and connect to the Internet with an application specific quality of service (QoS). For instance, public safety and autonomous driving applications require ultra-reliable-low-latency communications while monitoring and system automation may require massive number of connections with more flexible constraints in terms of latency and reliability. Therefore, developing a scalable wireless network that is able to accommodate the traffic generated from massively many nodes with different QoS requirements is mandatory to unleash the potential and benefits of the smart world era.

The access and reuse of wireless resources are fundamental challenges for MWNs. In the context of IoT, there are several evolving low-power wireless technologies, such as LoRa, SigFox, On-Ramp Wireless, and Weightless, to address such challenges [3]. The 3GPP LTE standard also provides solutions for accommodating IoT traffic within the cellular networks such as device-to-device communications, machine-to-machine communications, and narrowband IoT (NB-IoT) [4]. Each of these technologies provides innovative solutions in terms of energy efficiency, spectrum sharing, and traffic prioritization to fulfill the diverse requirements of IoT applications. Due to its distributed nature and simple operation,uncoordinated multiple access (UMA) is crucial for all these technologies [3]–[6]. In particular, ALOHA-based protocols are largely used to either transmit data or request scheduling. Synchronous ALOHA is of particular interest due to its higher performance when compared to its asynchronous counterpart.[1] Nevertheless, the performance of UMA degrades as the number of nodes grows [3]–[5], which raises the following fundamental questions: i) how to determine the scalability of UMA in MWNs in terms of per-node traffic intensity, node density, and required transmission rate; and ii) how to design a MWN with guaranteed stability and target performance level for a given network percentile. The answers to these questions will shed lights over the scalability of UMA in MWNs, highlight its operational bottlenecks, and enable applications for massive IoT and CPSs.

A. Related work

Conventionally, multiple access and scheduling schemes are characterized and designed via mathematical models that involve interacting queues [10]–[15]. However, pessimistic collision models are often used and only networks with small size are studied. More realistic signal-to-interference-plus-noise ratio (SINR)-based two-queue interactions are investigated in [16] and [17]; however, a generalization to MWNs appears to be a daunting task. Integrated graph and queueing theory models for interacting queues are presented in [18] and [19]. However, such approaches do not capture the

Manuscript received December 18, 2017; revised October 28, 2018; accepted December 7, 2018; approved by IEEE/ACM TRANSACTIONS ON NETWORKING Editor E. Yeh. Date of publication April 11, 2019; date of current version June 14, 2019. This work was supported in part by FAR and the "5×1000" Young Researcher Mobility Project, University of Ferrara, Italy, in part by the KAUST Sensor Research Initiative under Award OSR-2015-SENSORS-2700, and in part by the National Science Foundation under Grant CCF-1525705. This paper was presented in part at the 2017 IEEE International Symposium on Wireless Communication Systems. *(Corresponding author: Giovanni Chisci.)*

G. Chisci and A. Conti are with the Department of Engineering and CNIT, University of Ferrara, 44121 Ferrara, Italy (e-mail: giovanni.chisci@unife.it; a.conti@ieee.org).

H. ElSawy is with the Electrical Engineering Department, King Fahd University of Petroleum and Minerals, Dhahran 31261, Saudi Arabia (e-mail: hesham.elsawy@kfupm.edu.sa).

M.-S. Alouini is with the Computer, Electrical and Mathematical Science and Engineering Division, King Abdullah University of Science and Technology, Thuwal 23955, Saudi Arabia (e-mail: slim.alouini@kaust.edu.sa).

M. Z. Win is with the Laboratory of Information and Decision Systems, Massachusetts Institute of Technology, Cambridge, MA 02139 USA (e-mail: moewin@mit.edu).

Digital Object Identifier 10.1109/TNET.2019.2892709

[1] Note that network synchronization is viable in cellular and GPS-supported MWNs such as NB-IoT [7], or through distributed network synchronization [8], [9].

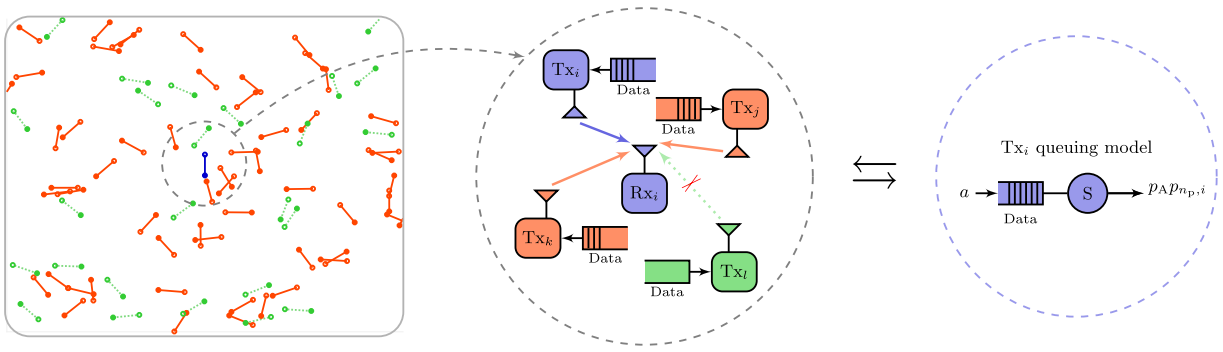

(a) Network Snapshot: active and inactive nodes

(b) Macroscopic scale: Interference from active nodes

(c) Microscopic scale: individual node activity

Fig. 1. Macroscopic and microscopic scales of the spatiotemporal model: in blue the intended link, in red other active links, and in green the inactive links.

aggregate effect from non-neighboring nodes, which may be significant in MWNs. In conclusion, previous models ignore the spatial and physical layer effects on queue interactions, which are fundamental in MWNs.

Spatial and physical layer attributes of wireless networks are usually captured via stochastic geometry models [20]–[25], where node positions are described according to point processes. Stochastic geometry based models account for radio propagation in conjunction with the theory of point processes to model concurrent transmissions that impose mutual interference among spatially coexisting nodes. However, the majority of stochastic geometry based models ignore temporal attributes such as traffic generation and queue occupation, as well as queueing key performance indicators (KPIs) such as latency and buffer occupation, all fundamental to characterize MWNs.

To jointly account for the spatial and temporal attributes of MWNs, recent studies combine stochastic geometry and queueing theory [26]–[32]. The spatiotemporal interactions between nodes with non-saturated data buffers are studied in [26]–[30]. However, the analysis in [26]–[28] assumes high mobility scenarios such that an independent realization of the network occur at every time slot. The spatiotemporal dynamics in static large scale networks is characterized in [29]–[31]. However, [29] and [31] utilizes a dominant system model where nodes in the network are always active even if they have empty queues in order to simplify the analysis, which can be quite pessimistic for MWNs. In [30], the uplink traffic for IoT-enabled cellular networks is analyzed, where every queue in the network behaves like the *typical queue*, which is not generally true for MWNs. The performance of UMA is characterized in [32] for static MWNs, which are the most challenging to analyze due to the spatiotemporal correlation of the interference at different locations. However, only UMA with single transmission power and *best-effort* traffic is considered. An alternative approach to characterize latency via bounds in static MWNs is proposed in [33], which is based on an integrated stochastic geometry and network calculus model.

B. Contribution

This paper presents a spatiotemporal model for UMA in MWNs, as depicted in Fig. 1(a).[2] The approach relies on the joint utilization of stochastic geometry and queueing theory. On the macroscopic scale, stochastic geometry is used to account for the mutual interference among active nodes (i.e., those with non-empty data buffer, as in Fig. 1(b)), which mainly depends on their position. On the microscopic scale, queueing theory is used to account for the per-node buffer state and transmission protocol state, which are determined by the traffic generation, UMA strategy, and link quality (see Fig. 1(c)). We also consider the intrinsic interdependency between the macroscopic- and microscopic-scale analysis, which enables an accurate characterization of link qualities by considering the aggregate interference from active nodes (i.e., accounting for the buffer and protocol states). The meta distribution of the SINR [37]–[40] is used to account for the diverse qualities of links coexisting in the network and to classify them into location-dependent QoS-classes. To this end, we quantify the network scalability via the γ-stability and γ-operativity Pareto frontiers, in which γ is a design parameter, in terms of per-node traffic intensity, node density, target transmission rate, and UMA persistence. Operating beyond the γ-stability frontier implies that the $(1-\gamma)$-percentile of the network operates with unstable queues, thus overflowing their data buffer. Analogously, beyond the γ-operativity frontier at least the $(1-\gamma)$-percentile of the network does not achieve the target KPI value (e.g., end-to-end latency or buffer size). This paper develops a framework to design networks with a guaranteed stability and a desired KPI value for a target percentile of the nodes in the MWN. The main contributions of this paper can be summarized as follows:

- develop a holistic mathematical model that accounts for the intricate spatiotemporal interactions in MWNs;
- present the γ-*stability* (γ-*operativity*) Pareto frontiers that guarantee stable queues (KPI value) for the γ-percentile of the MWN; and
- propose UMA strategies to balance the tradeoffs between transmission deferral, power-ramping, and persistence.

C. Notation and Organization

1) Notation: Along the paper we use the upright serif font, e.g., v, for random variables (RVs) and the italic roman font, e.g., v for their instantiation. Vectors are bolded, e.g., $\mathbf{v}$ and $\boldsymbol{v}$; matrices are bolded and uppercase, e.g., $\mathbf{V}$ and $\boldsymbol{V}$; and sets are uppercase, e.g., S and $\mathcal{S}$, as point processes, e.g., $\mathsf{\Pi}$ and $\mathit{\Pi}$. The notation $[\cdot]'$ is used to denote the transpose operator and $\boldsymbol{V}^{[i,j]}$ is used to denote the i^{th}-row j^{th}-column element. $\boldsymbol{V}^{[:,j]}$ and $\boldsymbol{V}^{[i,:]}$ are used to denote all elements in the j^{th} column and all elements in the i^{th} row, respectively. With a slight abuse of notation we use $v^{[i]}$ to denote the i^{th} element $\boldsymbol{v}^{[i]}$ of a vector. The functions $f_{\mathsf{v}}(\cdot)$, $F_{\mathsf{v}}(\cdot)$, and $\tilde{F}_{\mathsf{v}}(\cdot)$ denote the probability density function (PDF), cumulative distribution function (CDF), and complementary cumulative distribution function (CCDF) of the RV v, respectively. We denote by

[2]This work focus on synchronous systems, however can be generalized to asynchronous systems by modifying the stochastic geometry part according to [34]–[36] to account for partially overlapping transmissions in time.

$\mathbb{P}\{\cdot\}$, $\mathbb{E}\{\cdot\}$, $\mathbb{P}^{\circ}\{\cdot\}$, and $\mathbb{E}^{\circ}\{\cdot\}$ the probability, expectation, Palm probability, and Palm expectation with respect to (w.r.t.) the typical point, respectively. With the over-bar we denote the complement operator, i.e., $\bar{v} = 1 - v$; $\lceil\cdot\rceil$ denotes the ceiling function; and $\mathbb{1}_{\mathcal{S}}(n)$ is the indicator function, which assumes value one if $n \in \mathcal{S}$ and zero otherwise.

2) Organization: Section II presents the system model and the methodology; Section III shows the macroscopic analysis corresponding to the stochastic geometry part of the framework; Section IV delves into the microscopic analysis which corresponds to the queueing theory part of the framework; Section V develops the analysis framework for the spatiotemporal model and introduces the KPIs; Section VI presents numerical results; and, finally, Section VII provides the final remark.

II. System Model

A. Spatial and Physical Layer Parameters

This paper considers MWNs in which nodes are scattered in $\mathbb{R}^2$ according to a Poisson bipolar network (PBN) [41, Def. 5.8]. That is, the potential transmitters belong to a Poisson point process (PPP) $\Pi = \{\mathbf{y}_j \in \mathbb{R}^2, j \in \mathbb{N}^+\}$, with intensity λ and each transmitter communicates with a dedicated receiver located at a fixed distance R in a uniformly random direction. A realization of the PBN is shown in Fig. 1(a). For simplicity, we consider the unbounded path loss model $\ell(r) = r^{2\eta}$, where r is the propagation distance and η is the amplitude loss exponent. We consider zero-mean additive white Gaussian noise (AWGN) with average power σ^2 and a Rayleigh fading with unitary mean power gain. All channel gains are independent and identically distributed (IID) in space and time. Each transmission is defined by a frequency band and power level pair. Uniformly random channel selection among a common set of N_{c} frequency channels is adopted at each channel access, which is denoted as frequency ALOHA (F-ALOHA) [42]. The transmission power is selected among N_{p} different power levels in the set $\mathcal{P} = \{P_1, P_2, \ldots, P_{N_{\mathrm{p}}}\}$ according to the power-ramping scheme detailed in the following.

B. Temporal and MAC Layer Parameters

We consider a synchronized discrete-time system with slot duration of T_{s} seconds. As shown in Fig. 1(b), each transmitter has a buffer that stores data received from higher layers. An IID Bernoulli traffic generation model, with per-slot packet arrival probability of $a \in (0, 1]$, is assumed at each buffer.[3] At each time slot, transmitters with non-empty buffers employ the F-ALOHA protocol with probability $p_{\mathrm{fa}} \triangleq p_{\mathrm{a}}/N_{\mathrm{c}}$ to access one of the N_{c} channels, where p_{a} is the ALOHA transmission probability. Upon accessing a channel with bandwidth W [Hz], each transmitter operates at a fixed rate of $R_{\mathrm{t}} = W \log(1 + \theta)$ [bits/second]. Hence, a packet of size $T_{\mathrm{s}} R_{\mathrm{t}}$ [bits/packet] is successfully transmitted if the SINR at the intended receiver is equal to or greater than θ.

Packets are transmitted according to a first-in-first-out (FIFO) rule and only successfully received packets are dropped from the transmitter buffers. Otherwise, the packet is kept in the buffer until its successful transmission.[4]

[3]Bernoulli traffic arrival is a simple and widely accepted traffic model [29], [31]. Other traffic generation models can be adopted at the cost of more involved queueing theory analysis as described in Section IV.

[4]Positive and negative acknowledgement packets are sent instantaneously over an error-free control channel.

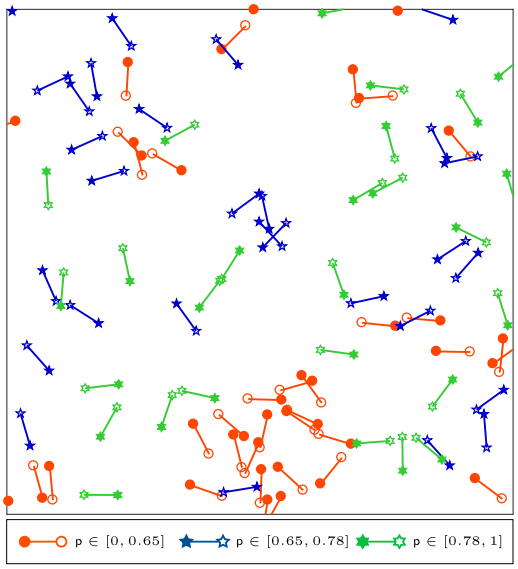

Fig. 2. Three QoS-classes classification for the TSP within a realization of the PBN operating with ALOHA for $N_{\mathrm{c}} = N_{\mathrm{p}} = N_{\mathrm{t}} = 1$ where the filled (empty) shapes represent transmitters (receivers).

When a transmission failure occurs, the node changes the transmission power at the next channel access according to the employed power-ramping scheme. A node uses the same transmission power P_i with $i \in \{1, 2, \ldots, N_{\mathrm{p}}\}$ (starting from the initial power level P_1) for up to N_{t} consecutive retransmissions,[5] where N_{t} is a design parameter. If the transmission is still unsuccessful, the next power level P_{i+1} is utilized for the next N_{t} retransmissions. We consider two power-ramping schemes, i.e., ramping-up and ramping-down. Ramping-up (i.e., $P_{i+1} > P_i$) is a greedy choice to prioritize delayed transmissions at the expense of increasing the interference level and deteriorating the transmission success probability (TSP) of other nodes' packets. In contrast, ramping-down ($P_{i+1} < P_i$) is an altruistic choice that reliefs the interference level in the network, especially in regions where packets are subjected to high latencies.[6] The retransmission protocol is restarted either upon a transmission success or after exploring all power levels (i.e., the counter tracking the retransmissions is cleared and the node restarts the transmission from P_1). The employed power-ramping protocol encompasses a total of $M = N_{\mathrm{p}} N_{\mathrm{t}}$ *transmission phases*, which are classified into N_{p} *physical phases* of different power levels and N_{t} *logical phases* for per-power level retransmissions.

Since the time scale of fading and packet transmission is much smaller than that of the spatial dynamics, it is assumed that the network realization remains static over a sufficiently large number of time slots. That is, an arbitrary, but fixed, network realization $\Pi = \mathit{\Pi}$ of the PBN is considered over the temporal domain while channel fading, queue states, node activities, channel access, and transmission powers change from one time slot to another.

C. Methodology

Network operation involves intricate and interdependent temporal interactions among the spatially distributed queues.

[5]Note that consecutive retransmissions do not necessarily occur in consecutive time slots due to the ALOHA random backoff.

[6]The proposed ramping scheme is based on the acknowledgments. More sophisticated channel-aware and coordinated power control schemes are left for future extensions.

As shown in Fig. 1, the macroscopic effect of the network interference and the microscopic effect of the per-node behavior are interrelated. Furthermore, the static network topology leads to a location-dependent packet departure probability of each queue, as depicted in Fig. 2, where nodes at sparse locations are more likely to have successful transmissions while nodes at congested locations are more likely to experience transmission failures. For a given link, the packet departure probability depends on i) the location of the intended receiver relative to the other transmitters, ii) the power employed by the intended transmitter, and iii) the status of all other transmitters (i.e., node activity and transmission power). For a given network realization $\Pi = \mathit{\Pi}$, let $n_{\mathrm{p}} \in \mathcal{N}_{\mathrm{p}} = \{1, 2, \ldots, N_{\mathrm{p}}\}$ be the power level index and $\mathsf{z}_{n_{\mathrm{p}},j}$ be the SINR at the intended receiver of the transmitter located at $\boldsymbol{y}_j \in \mathit{\Pi}$ when operating with the power level $P_{n_{\mathrm{p}}}$. Further, let $p_{n_{\mathrm{p}},j} \triangleq \mathbb{P}\{\mathsf{z}_{n_{\mathrm{p}},j} > \theta | \Pi = \mathit{\Pi}\}$ be the TSP of node j. A departure from the queue of the j^{th} wireless link occurs upon the joint independent events of channel access (any of the N_{c} available) and transmission success, i.e., with probability $p_{\mathrm{a}} p_{n_{\mathrm{p}},j}$. For any fixed $\Pi = \mathit{\Pi}$, the values $p_{n_{\mathrm{p}},j}$ along the network are realizations of the RV $\mathsf{p}_{n_{\mathrm{p}}}$. The distribution of the TSP $\mathsf{p}_{n_{\mathrm{p}}}$ across the network is denoted as the meta distribution of the SINR with CCDF $\bar{F}_{\mathsf{p}_{n_{\mathrm{p}}}}(\phi) \triangleq \mathbb{P}^{\circ}\{\mathsf{p}_{n_{\mathrm{p}}} > \phi\}$ which indicates the fraction of links in the network successfully transmitting with a probability greater than ϕ [37]. To obtain the meta distribution it is necessary to account for node activities (i.e., physical phases), which are modeled by the IID RVs $\mathsf{p}_j \in \mathcal{P} \cup \{0\}$ for $j \in \mathbb{N}^+$ with identical distributions $\boldsymbol{w} = [w^{[0]}, w^{[1]}, \ldots, w^{[N_{\mathrm{p}}]}]$ where $w^{[0]}$ is the probability of empty buffer (i.e., physical phase 0) and $w^{[i]}$ is the probability of having non-empty buffer while being in any of the retransmissions (i.e., logical phases) of the power level P_i (i.e., physical phase i).[7] Furthermore, to obtain the distribution $\boldsymbol{w}$ by an averaging step over all the location-dependent distributions of node physical phases, it is necessary to solve a finite number of queueing theory problems each of which require a TSP value drawn from the meta distribution. Thus, there is a coupling between the macroscopic and microscopic scale problems which is circumvented by using an iterative solution. To analyze a MWN, we utilize the following steps also depicted in Fig. 3.

(a) Macroscopic analysis via stochastic geometry
- For every power level $n_{\mathrm{p}} \in \mathcal{N}_{\mathrm{p}}$, find the statistical moments of $\mathsf{p}_{n_{\mathrm{p}}}$ as a function of $\boldsymbol{w}$, where the b^{th} moment is denoted by $M_{b,n_{\mathrm{p}}}$.
- For every power level $n_{\mathrm{p}} \in \mathcal{N}_{\mathrm{p}}$, approximate the PDF $f_{\mathsf{p}_{n_{\mathrm{p}}}}(\cdot)$ via the beta distribution having moments $M_{1,n_{\mathrm{p}}}$ and $M_{2,n_{\mathrm{p}}}$.
- For every power level $n_{\mathrm{p}} \in \mathcal{N}_{\mathrm{p}}$, discretize the PDF $f_{\mathsf{p}_{n_{\mathrm{p}}}}(\cdot)$ into N equiprobable values each corresponding to a QoS-class, i.e., $\boldsymbol{d}_{n_{\mathrm{p}}} = [d_{n_{\mathrm{p}}}^{[1]}, d_{n_{\mathrm{p}}}^{[2]}, \ldots, d_{n_{\mathrm{p}}}^{[N]}]$.
- Construct the TSP matrix $\boldsymbol{D}^{[n_{\mathrm{p}},i]} = p_{\mathrm{a}} d_{n_{\mathrm{p}}}^{[i]}$, where each row of $\boldsymbol{D}$ contains the TSPs for all QoS-classes using the same power level $n_{\mathrm{p}} \in \mathcal{N}_{\mathrm{p}}$ and each column contains the TSPs for all power levels within the same QoS-class $n \in \mathcal{N} = \{1, 2, \ldots, N\}$.

(b) Microscopic analysis via queueing theory
- For each QoS-class $n \in \mathcal{N}$, use the arrival probability a and the class dependent TSPs $\boldsymbol{D}^{[:,n]}$ to find the marginal steady-state distribution $\boldsymbol{\pi}_n = [\pi_n^{[0]}, \pi_n^{[1]}, \ldots, \pi_n^{[N_{\mathrm{p}}]}]$ of node physical phases, where $\pi_n^{[0]}$ is the probability of empty buffer and $\pi_n^{[n_{\mathrm{p}}]}$ is the probability of being in a retransmission phase that employs the power level n_{p}.
- Aggregate the per-class states to get the overall steady-state marginal distribution $\boldsymbol{w}$ of node physical phases, where $w^{[i]} = \frac{1}{N} \sum_{n=1}^{N} \pi_n^{[i]}$.

(c) Iterative solution
- Initialize $\boldsymbol{w}$ such that $\sum_{i=0}^{N_{\mathrm{p}}} w^{[i]} = 1$.
- Iterate (a) and (b) as in Fig. 3 until convergence.

[7] In the paper some distributions are given in the form of a stochastic vector, of which components sum up to one.

III. Macroscopic Stochastic Geometry Analysis

To characterize packet departures from the spatially interacting queues of Fig. 1 it is necessary to characterize the location-dependent TSP across the network (see Fig. 2).

Consider the point process of the transmitters with activity marks, i.e., $\dot{\Pi} = \{\mathsf{y}_j, \mathsf{a}_j, \mathsf{p}_j; j \in \mathbb{N}^+\}$ where marks a_j are IID Bernoulli RVs with probability $p_{\mathrm{fa}} = p_{\mathrm{a}}/N_{\mathrm{c}}$, due to the F-ALOHA channel access scheme, and $\mathsf{p}_j \in \mathcal{P} \cup \{0\}$ are discrete marks of the node physical phases. The marks a_j, for $j \in \mathbb{N}^+$, are independent due to the random channel selection and independent ALOHA transmissions. In contrast, the marks p_j are spatially and temporally correlated due to the static network topology that leads to location-dependent SINRs. As shown in Fig. 2, nodes at sparse locations have frequent successful transmissions, thus emptying their queues and being less likely to explore all the power levels provided by the protocol described in Sec. II-B. On the other hand, nodes at congested locations are more likely to have transmission failures, thus accumulating packets in their queues and exploring all power levels due to several retransmissions. Such a spatiotemporal correlation between node transmission phases complicates the analysis and necessitates the introduction of the following approximation, which will be further validated in Section VI.

Approximation 1 (Physical-Phase Marks IID Distribution): The marks p_j for all j are IID over different nodes and time slots according to the spatially averaged steady-state distribution $\boldsymbol{w} = [w^{[0]}, w^{[1]}, \ldots, w^{[N_{\mathrm{p}}]}]$.[8]

Remark 1: Approximation 1 is commonly known as *mean-field approximation* [26], [30], which ignores the spatiotemporal correlation between the physical phases of interfering nodes. Intuitively, the exact locations of interfering nodes and their correlated activities are of less significance to the SINR distribution at an intended receiver. Instead, the number (intensity) of the nodes employing each transmission power along with their relative locations with respect to the intended receiver are the main factors influencing the SINR, which are captured via the mean-field approximation.

The meta distribution of the SINR is characterized in the following by Approximation 1.

A. Meta Distribution Analysis

Let $\boldsymbol{y}_i \in \mathit{\Pi}$ and $\boldsymbol{y}_i^{\mathrm{rx}}$ be the locations of a transmitter and of its intended receiver, respectively. The TSP for the intended

[8] The spatially averaged steady-state distribution $\boldsymbol{w}$ is obtained in Section IV via queueing theory by averaging over all possible location-dependent distributions of the node physical phases.

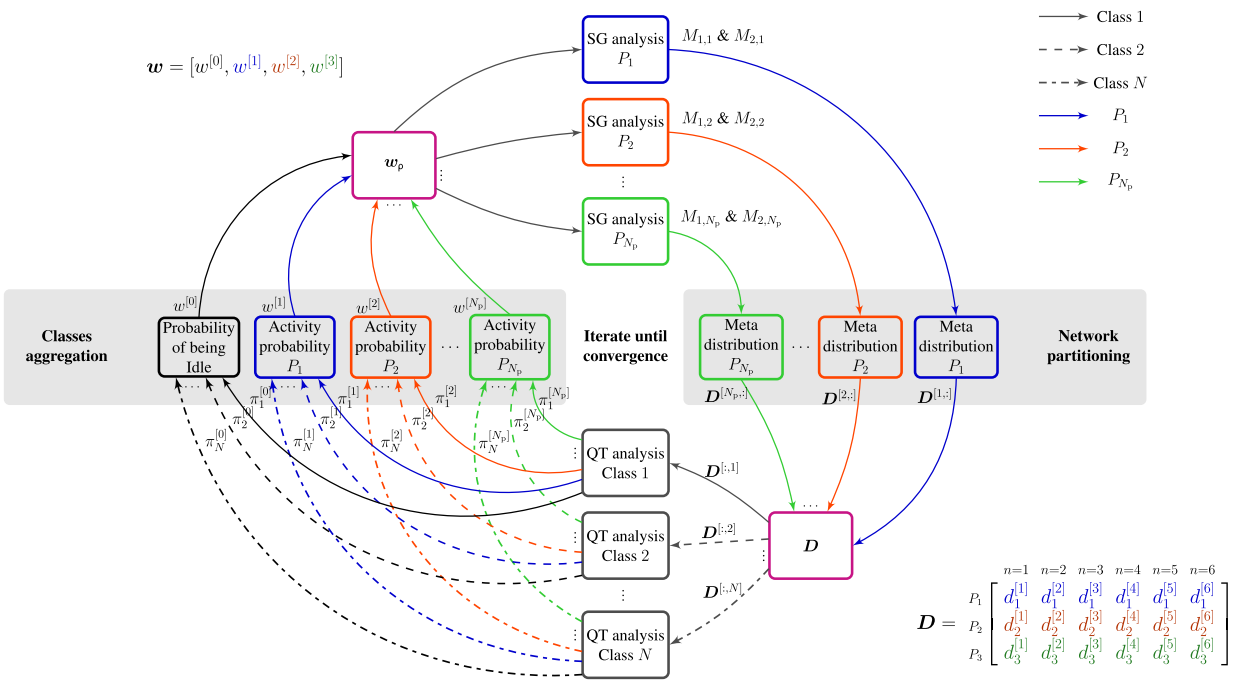

Fig. 3. Methodology of analysis and iterative algorithm within the proposed spatiotemporal model.

receiver can be characterized in terms of the transmission power and the marked PPP of interferers as

$$p_{n_\mathrm{p},i} \triangleq \mathbb{P}\{\mathsf{z}_{n_\mathrm{p},i} > \theta | \Pi = \mathit{\Pi}\} \tag{1a}$$

$$= \mathbb{P}\left\{ \frac{P_{n_\mathrm{p}} \mathsf{h}_i R^{-2\eta}}{\sum\limits_{j\,:\,\boldsymbol{y}_j \in \mathit{\Pi}\setminus\{\boldsymbol{y}_i\}} \mathsf{p}_j \mathsf{a}_j \mathsf{h}_j \|\boldsymbol{y}_j - \boldsymbol{y}_i^{\mathrm{rx}}\|^{-2\eta} + \sigma^2} > \theta \middle| \mathit{\Pi} \right\} \tag{1b}$$

where h_i is the channel gain of the intended link and σ^2 is the mean power of the zero-mean AWGN. Note that the relative locations of the interfering transmitters are fixed. However, the randomness in (1) is due to the spatiotemporal variation of fading, random channel selection, node activities, and transmission phases. In addition, due to the location-dependent interference seen by each receiver $\boldsymbol{y}_i^{\mathrm{rx}}$, $p_{n_\mathrm{p},i}$ across the network can be considered as realizations of the RV $\mathsf{p}_{n_\mathrm{p}}$ with CCDF $\tilde{F}_{\mathsf{p}_{n_\mathrm{p}}}(\phi)$, namely the meta distribution of the SINR. Such a meta distribution reveals the fraction of the network having a TSP greater than ϕ and, thanks to the ergodicity of the PPP, can be obtained via the Palm probability as $\tilde{F}_{\mathsf{p}_{n_\mathrm{p}}}(\phi) = \mathbb{P}^{\circ}\{\mathsf{p}_{n_\mathrm{p}} > \phi\}$ [37]. By following [37], the PDF of $\mathsf{p}_{n_\mathrm{p}}$ can be accurately approximated by the beta distribution as follows[9]

$$f_{\mathsf{p}_{n_\mathrm{p}}}(\phi) = \frac{\phi^{\frac{M_{1,n_\mathrm{p}}(\alpha+1)-1}{1-M_{1,n_\mathrm{p}}}} (1-\phi)^{\alpha-1}}{B\left(\frac{M_{1,n_\mathrm{p}}\alpha}{1-M_{1,n_\mathrm{p}}}, \alpha\right)} \tag{2}$$

with $\alpha = \frac{(M_{1,n_\mathrm{p}} - M_{2,n_\mathrm{p}})(1-M_{1,n_\mathrm{p}})}{M_{2,n_\mathrm{p}} - M_{1,n_\mathrm{p}}^2}$ where $B(\cdot,\cdot)$ is the complete beta function and the moments M_{1,n_p} and M_{2,n_p} are given in the following Theorem 1.

Theorem 1: The b^{th} order statistical moment of the TSP $\mathsf{p}_{n_\mathrm{p}}$ in a PBN as described in Section II is given by

$$M_{b,n_\mathrm{p}} \triangleq \mathbb{E}^{\circ}\{\mathsf{p}_{n_\mathrm{p}}^b\} = e^{-b\,\theta_{n_\mathrm{p}}\sigma^2} \exp\{-\lambda \nu_{b,n_\mathrm{p}}\} \tag{3}$$

[9]An exact but complex integral expression for the meta distribution can be obtained via Gil-Pelaez inversion theorem. However, it is shown in [37] that the beta approximation via moment matching is very tight, which highly simplifies the subsequent analysis and computations.

with

$$\nu_{b,n_\mathrm{p}} = \frac{\pi}{\eta} \sum_{k=1}^{b} \binom{b}{k} (-1)^{k+1} \int_0^\infty \left(p_{\mathrm{fa}} \sum_{i=1}^{N_\mathrm{p}} \frac{w^{[i]} \theta_{n_\mathrm{p},i}}{u + \theta_{n_\mathrm{p},i}} \right)^k u^{\frac{1-\eta}{\eta}} du \tag{4}$$

where $\theta_{n_\mathrm{p}} = \theta R^{2\eta}/P_{n_\mathrm{p}}$, $\theta_{n_\mathrm{p},i} = \theta_{n_\mathrm{p}} P_i$, and $w^{[i]}$ is the i^{th} element in $\boldsymbol{w}$. Let $\kappa = \pi\Gamma(1-\frac{1}{\eta})\Gamma(1+\frac{1}{\eta})\theta^{\frac{1}{\eta}} R^2$, the first moment of $\mathsf{p}_{n_\mathrm{p}}$ can be written as

$$M_{1,n_\mathrm{p}} = e^{-b\,\theta_{n_\mathrm{p}}\sigma^2} \exp\left\{ -\kappa \lambda p_{\mathrm{fa}} \sum_{i=1}^{N_\mathrm{p}} w^{[i]} \left(\frac{P_i}{P_{n_\mathrm{p}}} \right)^{\frac{1}{\eta}} \right\}. \tag{5}$$

In case of $N_\mathrm{p} = 1$ (single-transmission-power scheme) the integral expression in (4) reduces to the following closed forms for $b = 1, 2$ respectively as

$$M_1 = e^{-\,\theta_1 \sigma^2} \exp\{-\kappa \lambda p_{\mathrm{fa}} \tilde{w}^{[0]}\} \tag{6a}$$

$$M_2 = e^{-2\,\theta_1 \sigma^2} \exp\left\{ -2\kappa \lambda p_{\mathrm{fa}} \tilde{w}^{[0]} \left(1 - \frac{p_{\mathrm{fa}} \tilde{w}^{[0]}}{2} \left(1 - \frac{1}{\eta}\right)\right)\right\} \tag{6b}$$

where $\tilde{w}^{[0]} = 1 - w^{[0]}$.

Proof: See Appendix. □

Remark 2: The simplified expressions in (6) show that the spatially averaged TSP is exponentially decreasing in λ, p_{fa}, and $\tilde{w}^{[0]}$. Hence, having less traffic per node (i.e., higher probability of empty buffer) or more channels to access can significantly improve the TSP. Furthermore, (6) reveals that given the constant product λp_{a}, for $\lambda \to \infty$ and $p_{\mathrm{a}} \to 0$ then $M_2 \to M_1^2$, thus reducing the variance of $\mathsf{p}_{n_\mathrm{p}}$. This means that the TSP becomes location-independent.

The expression in (5) shows the positive impact of ramping up P_{n_p} for the intended link. However, it also captures the negative impact of ramping up the power of interfering nodes $w^{[i]} P_i^{\frac{1}{\eta}}$. Thus, power ramping has a dual effect, which is discussed in more detail in Section VI.

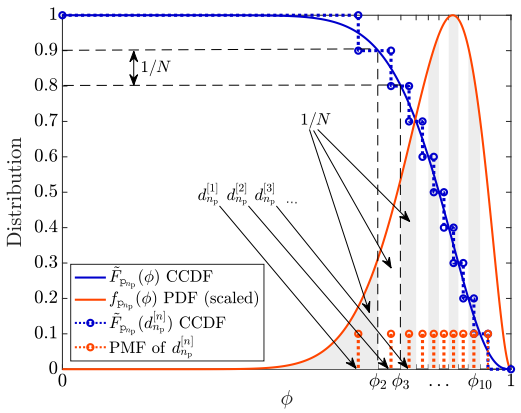

Fig. 4. Quantization of the distribution of the TSP for $N = 10$.

B. Network Uniform Partitioning

Consider that the PBN links are divided into different QoS-classes, each according to its location-dependent TSP (or equivalently queue departure probability). If each possible value of the continuous RV $\mathsf{p}_{n_\mathrm{p}}$ is considered as a TSP, then, an infinite number of QoS-classes are required to characterize the location-dependent performance of the nodes. For tractability, we partition the network into N QoS-classes by resorting to the following approximation.

Approximation 2 (Meta Distribution Quantization): Chose $N \in \mathbb{N}$ and quantize the continuous RV $\mathsf{p}_{n_\mathrm{p}}$ with distribution $f_{\mathsf{p}_{n_\mathrm{p}}}(\phi)$ as in (2) to the uniform discrete RV $\mathsf{d}_{n_\mathrm{p}} \in \boldsymbol{d}_{n_\mathrm{p}} = [d_{n_\mathrm{p}}^{[1]}, d_{n_\mathrm{p}}^{[2]}, \ldots, d_{n_\mathrm{p}}^{[N]}]$ where each value has probability $1/N$ [43]. The elements of $\boldsymbol{d}_{n_\mathrm{p}}$ are selected such that the mean error

$$\mathbb{E}_{\mathsf{p}_{n_\mathrm{p}}}\{\arg\min_n \|d_{n_\mathrm{p}}^{[n]} - \mathsf{p}_{n_\mathrm{p}}\|\} = \int_0^1 f_{\mathsf{p}_{n_\mathrm{p}}}(\phi) \arg\min_n \|d_{n_\mathrm{p}}^{[n]} - \phi\| \, d\phi$$

is minimized. The procedure is described in Algorithm 1 and illustrated in Fig. 4. The process is repeated for all $n_\mathrm{p} \in \mathcal{P}$ and the number of classes is selected to achieve sufficient accuracy in the description of the distributions of the TSP.

As shown in Algorithm 1, the $N_\mathrm{p} \times N$ matrix $\boldsymbol{D}$ can be constructed by using the vectors $\boldsymbol{d}_{n_\mathrm{p}}$ corresponding to each power level. The element $\boldsymbol{D}^{[i,j]} = d_i^{[j]}$ defines the TSP of the queue representing a link of the j^{th} QoS-class when the intended transmitter operates with power level P_i. As shown in Fig. 3, the matrix $\boldsymbol{D}$ of TSPs represents the interface between the stochastic geometry and the queueing theory analyses. An example of the network partitioning proposed in this section is illustrated in Fig. 2 for a single power level, i.e., $N_\mathrm{p} = 1$, and $N = 3$ QoS-classes. Since only a single power level is considered, TSPs are given in the 1×3 vector $\boldsymbol{d} \in \{d^{[1]} = 0.56, d^{[2]} = 0.71, d^{[3]} = 0.84\}$, such that each value represents $1/3$ of the PBN links.

IV. Microscopic Queueing Theory Analysis

To address the microscopic-scale analysis, each wireless link of the PBN, (e.g., that belonging to the n^{th} QoS-class) is considered as a queueing system (see Fig. 1) that is modeled via a discrete-time Markov chain (DTMC) to track the number

Algorithm 1 Meta distribution quantization

Require: N, M_{1,n_p}, and M_{2,n_p}.

Ensure: A TSP vector $\boldsymbol{d}_{n_\mathrm{p}}$ such that (s.t.) $F_{\mathsf{p}_{n_\mathrm{p}}}(d_{n_\mathrm{p}}^{[n]}) - F_{\mathsf{p}_{n_\mathrm{p}}}(d_{n_\mathrm{p}}^{[n+1]}) = 1/N$ for all $n_\mathrm{p} \in \mathcal{N}_\mathrm{p}$ and $n \in \mathcal{N} \setminus \{N\}$.

for $n_\mathrm{p} = 1, 2, \ldots, N_\mathrm{p}$ **do**
  Consider $f_{\mathsf{p}_{n_\mathrm{p}}}(\phi)$ by (2);
  Set $\phi_1 = 0$ and $\phi_{N+1} = 1$;
  for $n = 1, 2, \ldots, N-1$ **do**
    Retrieve the values of ϕ_n and ϕ_{n+1} s.t.

$$F_{\mathsf{p}_{n_\mathrm{p}}}(\phi_n) - F_{\mathsf{p}_{n_\mathrm{p}}}(\phi_{n+1}) = \int_{\phi_n}^{\phi_{n+1}} f_{\mathsf{p}_{n_\mathrm{p}}}(\phi)\, d\phi = \frac{1}{N}$$

    Compute $d_{n_\mathrm{p}}^{[n]}$ s.t.

$$\int_{\phi_n}^{d_{n_\mathrm{p}}^{[n]}} f_{\mathsf{p}_{n_\mathrm{p}}}(\phi)\, d\phi = \int_{d_{n_\mathrm{p}}^{[n]}}^{\phi_{n+1}} f_{\mathsf{p}_{n_\mathrm{p}}}(\phi)\, d\phi = \frac{1}{2N};$$

  end for
  Assign $\boldsymbol{D}^{[n_\mathrm{p},:]} = \boldsymbol{d}_{n_\mathrm{p}}$ and $f_{\mathsf{d}_{n_\mathrm{p}}}(d_{n_\mathrm{p}}^{[n]}) = 1/N$;
end for
Return $\boldsymbol{D}$.

of packets l_n in the transmitter buffer, the physical power-level phase, and the logical retransmission phase (see Fig. 5). As discussed in Section III, the location-dependent performance of nodes leads to temporally correlated packet departure probabilities for each queue (see Figs. 2 and 4). To capture such location-dependence while avoiding queueing memory complications, we resort to the following approximation.

Approximation 3 (QoS-Aware But Temporally-Independent Departure Rates): Recall that $\boldsymbol{D}$ is the TSP matrix obtained by discretizing the meta distribution of the SINR in Algorithm 1. At a generic time slot, the departure probability of a packet from a queue that belongs to the n^{th} QoS-class and operates with power P_{n_p} is given by $p_\mathrm{a}\boldsymbol{D}^{[n_\mathrm{p},n]}$. A queue does not change its QoS-class over time. The departures from the same queue in different time slots with transmission powers P_{n_p} and $P_{n'_\mathrm{p}}$ are considered to be independent with probabilities $p_\mathrm{a}\boldsymbol{D}^{[n_\mathrm{p},n]}$ and $p_\mathrm{a}\boldsymbol{D}^{[n'_\mathrm{p},n]}$, respectively.

Approximation 3 suggests that the mean departure probability of each queue is determined by its static location, which does not change over a sufficiently large number of time slots. However, the departure probability from each queue is still random and independent from one time slot to another due to the independent random variations of the channel gains, of the interfering nodes' activities, and of transmission powers. Based on Approximation 3, the queueing model for each link is represented via a Geo/Ph/1 DTMC [44, Ch. 5.8] with the QoS-class dependent state diagram shown in Fig. 5, where the packet departure probabilities are given by $p_\mathrm{a}\boldsymbol{D}^{[:,n]}$. In Geo/Ph/1 queues, the *phase type distribution* [44, Ch. 2.5.3] of departures is constructed via an absorbing Markov chain [44, Ch. 3.4.4] that accounts for all the transmission phases that a queue belonging to a given QoS-class may experience until a packet departure.[10] To build the transition matrix of

[10]In the absorbing Markov chain, the absorption denotes successful transmission. $\boldsymbol{S}_n$ in (8) define the dynamic of the phases before absorption.

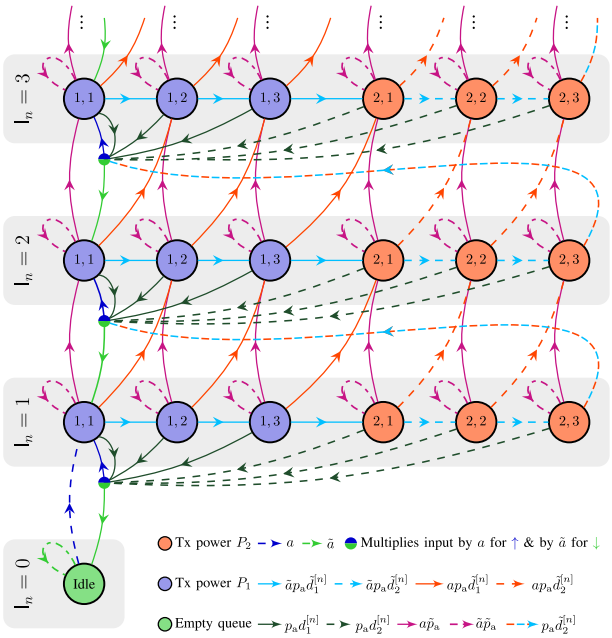

Fig. 5. The DTMC for a class n queue with two power levels $\mathcal{P} = \{P_1, P_2\}$ and $N_\mathrm{t} = 3$ retransmissions for each power level.

the considered Geo/Ph/1 DTMC, we first define the following $N_\mathrm{t} \times N_\mathrm{t}$ matrices,

$$\boldsymbol{H}_{n_\mathrm{p},n}^{[i,j]} = \begin{cases} \tilde{p}_\mathrm{a} & \text{if } i = j \\ p_\mathrm{a}\tilde{\boldsymbol{D}}^{[n_\mathrm{p},n]} & \text{if } j = i+1 \\ 0 & \text{otherwise} \end{cases} \tag{7a}$$

$$\boldsymbol{J}_{n_\mathrm{p},n}^{[i,j]} = \begin{cases} p_\mathrm{a}\tilde{\boldsymbol{D}}^{[n_\mathrm{p},n]} & \text{if } i = N_\mathrm{t} \text{ and } j = 1 \\ 0 & \text{otherwise} \end{cases} \tag{7b}$$

where $\tilde{p}_\mathrm{a} = 1 - p_\mathrm{a}$ and $\tilde{\boldsymbol{D}}^{[n_\mathrm{p},n]} = 1 - \boldsymbol{D}^{[n_\mathrm{p},n]}$. The (7a) contains the probabilities of ALOHA deferral and horizontal transition between the logical phases (i.e., retransmissions) within the same power level, while (7b) contains the probabilities of horizontal transition from one power level to the next. Given that there are N_p different power levels with N_t retransmissions within each power level, the transient state sub-stochastic matrix for the absorbing Markov chain is given by the following block matrix

$$\boldsymbol{S}_n = \begin{bmatrix} \boldsymbol{H}_{1,n} & \boldsymbol{J}_{1,n} & & & \\ & \boldsymbol{H}_{2,n} & \boldsymbol{J}_{2,n} & & \\ & & \ddots & \ddots & \\ & & & \boldsymbol{H}_{N_\mathrm{p}-1,n} & \boldsymbol{J}_{N_\mathrm{p}-1,n} \\ \boldsymbol{J}_{N_\mathrm{p},n} & & & & \boldsymbol{H}_{N_\mathrm{p},n} \end{bmatrix} \tag{8}$$

where the empty blocks are filled by zeroes. The $M \times M$ matrix $\boldsymbol{S}_n$, where $M = N_\mathrm{p}N_\mathrm{t}$, accounts for all power levels and retransmission phases until a packet is successfully transmitted (i.e., absorption). In case of F-ALOHA with no power ramping (i.e., $M = N_\mathrm{p} = N_\mathrm{t} = 1$) the transient state sub-stochastic matrix is simply given by $\boldsymbol{S}_n = \boldsymbol{H}_n + \boldsymbol{J}_n$. The absorption probabilities from each transient state phase is defined by the M-sized vector

$$\boldsymbol{s}_n = \mathbf{1} - \boldsymbol{S}_n\mathbf{1} = [s_n^{[1]}, s_n^{[2]}, \ldots, s_n^{[M]}]' \tag{9a}$$

where $\mathbf{1}$ is a column vector of ones of the proper size and $s_n^{[m]}$ is the probability that a packet is transmitted and successfully decoded within a link of class n for a transmitter in phase $m = (n_\mathrm{p} - 1)N_\mathrm{t} + n_\mathrm{t}$. The index n_p of the transmission power used by the intended transmitter can be retrieved from m as $n_\mathrm{p} = \lceil m/N_\mathrm{t} \rceil$ and, hence, $s_n^{[m]} = p_\mathrm{a} d_{n_\mathrm{p}}^{[n]}$.[11] Since the transmission of each new packet starts with power $n_\mathrm{p} = 1$ and $n_\mathrm{t} = 1$, the initialization vector for the absorbing Markov chain is $\boldsymbol{\beta} = [1, 0, \ldots, 0] \in \mathbb{R}^{M\times 1}$.

By considering $\boldsymbol{S}_n$, $\boldsymbol{s}_n$, and $\boldsymbol{\beta}$, the DTMC of the n^{th} QoS-class link is dedscribed by a quasi-birth-and-death (QBD) process [44] with the following block transition matrix

$$\boldsymbol{P}_n = \begin{array}{c} \\ \mathsf{l}_n{=}0 \\ \mathsf{l}_n{=}1 \\ \mathsf{l}_n{=}2 \\ \mathsf{l}_n{=}3 \\ \vdots \end{array} \begin{array}{c} \begin{array}{ccccccc} \mathsf{l}_n{=}0 & \mathsf{l}_n{=}1 & \mathsf{l}_n{=}2 & \mathsf{l}_n{=}3 & \mathsf{l}_n{=}4 & \cdots \end{array} \\ \begin{bmatrix} \boldsymbol{B}_n & \boldsymbol{C}_n & & & & \\ \boldsymbol{E}_n & \boldsymbol{A}_{1,n} & \boldsymbol{A}_{0,n} & & & \\ & \boldsymbol{A}_{2,n} & \boldsymbol{A}_{1,n} & \boldsymbol{A}_{0,n} & & \\ & & \boldsymbol{A}_{2,n} & \boldsymbol{A}_{1,n} & \boldsymbol{A}_{0,n} & \\ & & & \ddots & \ddots & \ddots \end{bmatrix} \end{array} \tag{10}$$

where l_n represents the different levels (i.e., number of packets in the queue) within a generic n^{th} class queue, $\boldsymbol{B}_n = \tilde{a} \in \mathbb{R}$, $\boldsymbol{E}_n = \tilde{a}\boldsymbol{s}_n \in \mathbb{R}^{M\times 1}$, $\boldsymbol{C} = a\boldsymbol{\beta} \in \mathbb{R}^{1\times M}$, $\boldsymbol{A}_{0,n} = a\boldsymbol{S}_n \in \mathbb{R}^{M\times M}$, $\boldsymbol{A}_{1,n} = a\boldsymbol{s}_n\boldsymbol{\beta} + \tilde{a}\boldsymbol{S}_n \in \mathbb{R}^{M\times M}$, $\boldsymbol{A}_{2,n} = \tilde{a}\boldsymbol{s}_n\boldsymbol{\beta} \in \mathbb{R}^{M\times M}$, and the empty blocks are filled by zeroes. The steady-state distribution of a queue with transition matrix $\boldsymbol{P}_n$ is then obtained by solving the following system of equations

$$\boldsymbol{x}_n\boldsymbol{P}_n = \boldsymbol{x}_n \tag{11a}$$

$$\boldsymbol{x}_n\mathbf{1} = 1 \tag{11b}$$

where $\boldsymbol{x}_n = [x_n^{[0]}, \boldsymbol{x}_n^{[1]}, \boldsymbol{x}_n^{[2]}, \ldots, \boldsymbol{x}_n^{[l]}, \ldots]$ is the steady-state probability vector for all levels $l = 1, 2, \ldots$ of the n^{th} QoS-class queue; $x_n^{[0]}$ is the probability of empty buffer; $\boldsymbol{x}_n^{[l]} = [x_{l,n}^{[1]}, x_{l,n}^{[2]}, \ldots, x_{l,n}^{[M]}]$ is the distribution of phases in level l, and $x_{l,n}^{[m]}$ is the probability of being at level l and phase m.

Since the considered queueing model is ergodic and irreducible [44, Ch. 3.4.4], the system of equations in (11) has a unique solution if the queue is stable. To check the stability, we first construct the matrix $\boldsymbol{A}_n = \boldsymbol{A}_{0,n} + \boldsymbol{A}_{1,n} + \boldsymbol{A}_{2,n} = \boldsymbol{s}_n\boldsymbol{\beta} + \boldsymbol{S}_n$, and solve the system

$$\boldsymbol{\psi}_n\boldsymbol{A}_n = \boldsymbol{\psi}_n \tag{12a}$$

$$\boldsymbol{\psi}_n\mathbf{1} = 1 \tag{12b}$$

for $\boldsymbol{\psi}_n = [\psi_n^{[1]}, \psi_n^{[2]}, \ldots, \psi_n^{[M]}]$, which is the marginal distribution of all transmission phases when the buffer is non empty. The queue is stable if and only if (i.f.f.) [44]

$$\boldsymbol{\psi}_n\boldsymbol{A}_{2,n}\mathbf{1} > \boldsymbol{\psi}_n\boldsymbol{A}_{0,n}\mathbf{1}. \tag{13}$$

Condition (13) leads to two different types of analysis, namely stable-QoS-class and unstable-QoS-class analysis.

A. Stable-QoS-class Analysis

If the condition in (13) is satisfied, then the QoS-class represented by (11) is stable and has a unique solution. Then, using the systematic matrix analytic method (MAM) [44], the system in (11) has the following solution

$$x_n^{[0]} = \left(1 + \boldsymbol{C}\boldsymbol{T}\left(\boldsymbol{I} - \boldsymbol{R}_n\right)^{-1}\mathbf{1}\right)^{-1} \tag{14a}$$

$$\boldsymbol{x}_n^{[l]} = \begin{cases} x_n^{[0]}\boldsymbol{C}\boldsymbol{T} & \text{for } l = 1 \\ \boldsymbol{x}_n^{[1]}\boldsymbol{R}_n^{l-1} & \text{for } l > 1 \end{cases} \tag{14b}$$

[11] The superscript m is used for brevity where the specification of n_p and n_t is not needed. In general, a transmission phase is always associated with a single transmission power-retransmission index pair.

where $\boldsymbol{T} = \left(\boldsymbol{I} - a\boldsymbol{s}_n\boldsymbol{\beta} - \tilde{a}\boldsymbol{S}_n - \boldsymbol{R}_n\tilde{a}\boldsymbol{s}_n\boldsymbol{\beta}\right)^{-1}$, $\boldsymbol{I} \in \mathbb{R}^{M\times M}$ is the identity matrix and $\boldsymbol{R}_n \in \mathbb{R}^{M\times M}$ is the rate matrix given by $\boldsymbol{R}_n = a\boldsymbol{S}_n\boldsymbol{T}$. Let $\boldsymbol{\zeta}_n = [\zeta_n^{[1]}, \zeta_n^{[2]}, \ldots, \zeta_n^{[M]}]$ be the vector containing the probabilities of being in any transmission phase irrespective of the buffer level, then

$$\boldsymbol{\zeta}_n = \boldsymbol{x}_n^{[1]}(\boldsymbol{I} - \boldsymbol{R}_n)^{-1}. \tag{15}$$

Note that $\boldsymbol{\zeta}_n$ is a sub-stochastic vector[12] as it does not contain the probability of empty buffer. The steady-state marginal distribution for the powers levels $\boldsymbol{\pi}_n$ is given by

$$\pi_n^{[0]} = x_n^{[0]} \tag{16a}$$

$$\pi_n^{[n_\mathrm{p}]} = \sum_{m=1}^{M} \mathbb{1}_{\mathcal{M}}(m)\, \zeta_n^{[m]} \tag{16b}$$

where $\mathbb{1}_{\mathcal{M}}(m)$ equals one if $m \in \mathcal{M} = \{m' : \lceil m'/N_\mathrm{t} \rceil = n_\mathrm{p}\}$ and zero otherwise, which ensures that the sum is over the logical phases (i.e., retransmissions) within the same physical phase (i.e., transmission power) with index n_p.

B. Unstable-QoS-class Analysis

If the condition in (13) is not satisfied, then the QoS-class represented by (11) is unstable and the node buffers will overflow with probability one. In this case, the probability of empty buffer is zero, i.e., $x_n^{[0]} = 0$, and the marginal distribution of the phases is the one obtained from solving (12). Hence, the steady-state marginal distribution $\boldsymbol{\pi}_n$ for the power levels is given by

$$\pi_n^{[0]} = 0 \tag{17a}$$

$$\pi_n^{[n_\mathrm{p}]} = \sum_{m=1}^{M} \mathbb{1}_{\mathcal{M}}(m)\, \psi_n^{[m]}. \tag{17b}$$

C. Class Aggregation

As shown in Fig. 3, the class aggregation is the conjunction between the queueing theory and stochastic geometry analysis, thus computing the spatially averaged $\boldsymbol{w}$. From Approximation 1, the spatial and temporal correlations among the physical-phase marks of the interfering nodes are ignored and the aggregate interference is characterized assuming IID node physical-phase distribution $\boldsymbol{w}$.

Remark 3: We compute the IID node physical-phase distribution $\boldsymbol{w}$ of Approximation 1 by an average over the N equiprobable QoS-classes obtained by Approximation 2. For $i = 0, 1, \ldots, N_\mathrm{p}$ we have

$$w^{[i]} = \frac{1}{N}\sum_{n=1}^{N} \pi_n^{[i]}. \tag{18}$$

V. Analysis Framework

To characterize the network performance and obtain the KPIs, the coupling between the stochastic geometry and the queueing theory parts needs to be solved. Specifically, the TSP matrix $\boldsymbol{D}$ requires the spatially averaged physical-phase distribution $\boldsymbol{w}$. Meanwhile, $\boldsymbol{w}$ requires $\boldsymbol{D}$ to be computed. Before delving into the iterative solution, it is worth highlighting the necessary condition (NC) and sufficient condition (SC) for stability of each QoS-class.

[12]A sub-stochastic vector has components that are probabilities but it does not sum up to one.

A. Stability Conditions

According to Loynes theorem [45], a stable queue has the packet departure probability greater than the packet arrival probability, which guarantees finite mean buffer size and waiting time in queue. The NC and SC for stability can be obtained through the mildest and most severe interference scenarios, respectively. Note that NC and SC are computed directly and do not require any iterative solution. As an example, for a ramping-up strategy, the NC can be obtained by setting $\boldsymbol{w} = \boldsymbol{w}^{\mathrm{nc}} = [1-a, a, 0, \ldots, 0]$, which captures the mildest interference scenario by activating the nodes with fresh packets only. In contrast, the SC can be obtained by setting $\boldsymbol{w} = \boldsymbol{w}^{\mathrm{sc}} = [0, \ldots, 0, 1]$, which captures the most severe interference scenario where all nodes are active regardless of their buffer state as shown in the following corollary.

Corollary 1: Assuming an interference limited regime, the b^{th}-order moment of the TSP in the mildest and in the most severe interference scenarios are, respectively, given by

$$M_b^{\mathrm{nc}} = \exp\left\{\frac{\pi\lambda}{\eta}\sum_{k=1}^{b}\binom{b}{k}\int_0^{\infty}\left(\frac{ap_{\mathrm{fa}}\theta R^{2\eta}}{u+\theta R^{2\eta}}\right)^k \frac{(-1)^k}{u^{\frac{\eta-1}{\eta}}}\,du\right\} \tag{19a}$$

$$M_b^{\mathrm{sc}} = \exp\left\{\frac{\pi\lambda}{\eta}\sum_{k=1}^{b}\binom{b}{k}\int_0^{\infty}\left(\frac{p_{\mathrm{fa}}\theta R^{2\eta}}{u+\theta R^{2\eta}}\right)^k \frac{(-1)^k}{u^{\frac{\eta-1}{\eta}}}\,du\right\}. \tag{19b}$$

Proof: Follows directly from Theorem 1 by ignoring noise and assuming that all active transmitters operate with equal powers, and setting $\boldsymbol{w} = \boldsymbol{w}^{\mathrm{nc}}$ and $\boldsymbol{w} = \boldsymbol{w}^{\mathrm{sc}}$. □

By using M_b^{nc} and M_b^{sc}, the TSP matrices $\boldsymbol{D}^{\mathrm{nc}}$ and $\boldsymbol{D}^{\mathrm{sc}}$, respectively, can be constructed via Algorithm 1. By using $\boldsymbol{D}^{\mathrm{nc}}$ and $\boldsymbol{D}^{\mathrm{sc}}$, the NC and SC can be respectively verified for each QoS-class via condition (13). It is obvious that a satisfied SC condition implies a satisfied NC condition and that unsatisfied NC implies unsatisfied SC condition. Hence, the NC and SC verification lead to the following cases: i) both NC and SC are satisfied; ii) neither of NC and SC are satisfied; and iii) the NC is satisfied and the SC is unsatisfied. When both (neither) conditions are satisfied, then it can be directly concluded that the n^{th} QoS-class is stable (unstable). However, in the third case, further investigation through the iterative algorithm is required to check the stability of the n^{th} QoS-class.

B. Iterative Algorithm

The iterative algorithm used to find the steady state $\boldsymbol{w}$ is depicted in Fig. 3 and presented in Algorithm 2. The Algorithm 2 solves the fixed point equation $\boldsymbol{w} = g(\boldsymbol{w})$, where $\boldsymbol{w}$ is the steady-state averaged marginal distribution of the node physical phases. Starting from a valid stochastic vector $\boldsymbol{w}$, the function $g(\cdot)$ involves the steps described in Section II-C, depicted in Fig. 3, and particularized in Algorithm 2. Given the complicated and multi-stage nature of such fixed point equation, addressing the solution unicity and convergence is seldom possible.[13] For our model, the existence and unicity of the solution and the convergence of the iterative procedure

[13]The solution unicity and convergence were established for simpler models (e.g., only spatially averaged analysis and single transmission power) that involve iterative solution between stochastic geometry and queueing theory [26], [28].

Algorithm 2 Iterative solution (networks of Geo/Ph/1 queues)

Require: λ, $p_{\rm a}$, a, N, θ, η, R, σ^2, $N_{\rm c}$, $N_{\rm p}$, $N_{\rm t}$, $\mathcal{P}$, and $\boldsymbol{\beta}$.
Ensure: $\boldsymbol{D}$ and for all $n = 1, 2, \ldots, N$, $\boldsymbol{x}_n$ for stable classes and $\boldsymbol{\psi}_n$ for unstable classes.
Inizialize $k = 1$, $\epsilon \ll 1$, $\boldsymbol{w}^{[1]}$ s.t. $\boldsymbol{w}^{[1]}\mathbf{1} = 1$.
while $\max_n \{\|\boldsymbol{w}^{[k]} - \boldsymbol{w}^{[k-1]}\|\} \geq \epsilon$ **do**
  for $n_{\rm p} \in \mathcal{P}$ **do**
    Compute the moments $M_{1,n_{\rm p}}$, $M_{2,n_{\rm p}}$ by (3), (4);
    Run Algorithm 1 to populate $\boldsymbol{D}$;
  end for
  for $n \in \mathcal{N}$ **do**
    Construct $\boldsymbol{S}_n$ and $\boldsymbol{s}_n$ by (7), (8), and (9);
    Construct $\boldsymbol{A}_n = \boldsymbol{s}_n\boldsymbol{\beta} + \boldsymbol{S}_n$;
    Obtain $\boldsymbol{\psi}_n$ by solving (12);
    if $\boldsymbol{\psi}_n\boldsymbol{A}_{2,n}\mathbf{1} > \boldsymbol{\psi}_n\boldsymbol{A}_{0,n}\mathbf{1}$ **then**
      Queues of the $n^{\rm th}$ class are stable;
      Obtain $\boldsymbol{x}_n$ through (14);
      Evaluate $\boldsymbol{\pi}_n$ through (15) and (16)
    else
      Queues of the $n^{\rm th}$ class are unstable;
      Set $\pi_n^{[0]} = 0$ and use $\boldsymbol{\psi}_n$ to find $\boldsymbol{\pi}_n$ via (17);
    end if
  end for
  Calculate $\boldsymbol{w}^{[k+1]}$ by (18);
end while
Return $\boldsymbol{x}_n$ for stable classes, $\boldsymbol{\psi}_n$ for non-stable classes, $M_{1,n_{\rm p}}$, $M_{2,n_{\rm p}}$, and $\boldsymbol{D}$.

can be argued by the following facts: i) each legitimate $\boldsymbol{w}$ leads to a unique distribution of the TSP, and hence, a unique TSP matrix $\boldsymbol{D}$; ii) each TSP matrix $\boldsymbol{D}$ leads to a unique queueing steady-state solution $\boldsymbol{\pi}_n$ for each class; and iii) the fixed point equation operates over a stochastic vector (i.e., $0 \leq w^{[i]} \leq 1$, $0 \leq [g(\boldsymbol{w})]^{[i]} \leq 1$, $\boldsymbol{w}\mathbf{1} = 1$, and $[g(\boldsymbol{w})]\mathbf{1} = 1$) and the lefthand side $\boldsymbol{w}$ spans the entire multidimensional domain. It is worth highlighting that in case of satisfied NC but unsatisfied SC for a given QoS-class, there may exist two solutions for the queueing system steady-state probability vector $\boldsymbol{\pi}_n$. One solution has $\pi_n^{[0]} = 0$ (i.e., no empty buffers) due to the unsatisfied SC. The other solution would have $\pi_n^{[0]} > 0$ if there exists a steady-state configuration $\boldsymbol{w}$ that lead to a satisfied (13). Since the stable solution is the one of interest, we initialize $\boldsymbol{w}$ for $k = 1$ as $\boldsymbol{w}^{[1]} = [1-a, a, 0, \ldots, 0]$ in Algorithm 2. It is worth noting that the aforementioned arguments about convergence of Algorithm 2 are supported via extensive Monte Carlo simulation as shown in Section VI.

C. Network Stability

The network percentile that operates with stable queues is given by

$$\gamma_{\rm su} = \frac{1}{N}\sum_{n=1}^{N} \mathbb{1}_{\mathcal{S}}(n) \tag{20}$$

where $\mathcal{S} = \{n' : \boldsymbol{\psi}_{n'}\boldsymbol{A}_{2,n'}\mathbf{1} > \boldsymbol{\psi}_{n'}\boldsymbol{A}_{0,n'}\mathbf{1}\}$; and where $\boldsymbol{\psi}_n$, $\boldsymbol{A}_{2,n}$, and $\boldsymbol{A}_{0,n}$ are obtained from Algorithm 2 for every QoS-class after convergence. Note that (20) follows from the Loynes theorem along with the stability condition in (13).

Considering the space of the system parameters $\mathcal{R} = \{\lambda, \theta, a, p_{\rm a}, N_{\rm c}\} \in \mathcal{G} = [\mathbb{R}^+]^2 \times [0,1]^2 \times \mathbb{N}$ and the function $\gamma_{\rm su} : \mathcal{G} \to [0,1]$, we define the γ-*stability region* as

$$\mathcal{R}_\gamma^{\rm s} \triangleq \{\mathcal{R} : \gamma_{\rm su}(\mathcal{R}) > \gamma\} \tag{21}$$

i.e., as the region where a fraction of the nodes greater than γ operates with stable queues.[14] For a given $\mathcal{R}$, in addition to the de facto $\gamma_{\rm su}$ obtained through (20), the percentile of the PBN satisfying the NC and SC conditions can be obtained by utilizing Corollary 1 though the following steps: i) use $M_b^{\rm nc}$ and $M_b^{\rm sc}$ in Algorithm 1 to obtain, respectively, $\boldsymbol{D}^{\rm nc}$ and $\boldsymbol{D}^{\rm sc}$; ii) use $\boldsymbol{D}^{\rm nc}$ and $\boldsymbol{D}^{\rm sc}$ to construct the queueing model for each QoS-class and check (13); and iii) utilize (20) to obtain the percentile PBN satisfying the NC and SC conditions.

Remark 4: Since stability implies finite latency, $\gamma_{\rm su}$ is of particular interest for *best-effort* traffic, which requires eventual packet delivery and is tolerant to latency.

D. Key Performance Indicators

Algorithm 2 provides the steady-state probabilities (i.e., $\boldsymbol{x}_n$ and $\boldsymbol{\psi}_n$), the moments of the SINR (i.e., $M_{1,n_{\rm p}}$ and $M_{2,n_{\rm p}}$), and the TSP matrix $\boldsymbol{D}$, from which a variety of KPIs can be computed [46], [47]. For instance, following [44, Ch. 5.8] for Geo/Ph/1 queues, the *average number of packets in the system* and the *average buffer length* of a node that belongs to the $n^{\rm th}$ QoS-class are given, respectively, by

$$\bar{l}_n = \mathbb{E}\{\mathsf{l}_n\} = \boldsymbol{x}_n^{[1]}(\boldsymbol{I} - \boldsymbol{R})^{-2}\mathbf{1} \tag{22a}$$

$$\bar{q}_n = \mathbb{E}\{\mathsf{q}_n\} = \boldsymbol{x}_n^{[1]}\boldsymbol{R}(\boldsymbol{I} - \boldsymbol{R})^{-2}\mathbf{1}. \tag{22b}$$

Let t_n and $\mathsf{t}_{{\rm q}n}$ denote the total latency and the waiting time in the buffer (i.e., the number of time slots that a packet spends in the queue before the service starts), respectively. The *average total latency* and *average waiting time in the buffer* for the $n^{\rm th}$ class are provided by the discrete time version of the Little's law [46], respectively, as

$$\bar{t}_n = \mathbb{E}\{\mathsf{t}_n\} = \mathbb{E}\{\mathsf{l}_n\}/a \tag{23a}$$

$$\bar{t}_{{\rm q}n} = \mathbb{E}\{\mathsf{t}_{{\rm q}n}\} = \mathbb{E}\{\mathsf{q}_n\}/a. \tag{23b}$$

The service latency $\mathsf{t}_{\rm s}$ (i.e., the number of time slots required to complete the transmission once a packet arrives at the head of the buffer) accounts for ALOHA transmission deferrals and transmission failures due to the event $\{SINR \leq \theta\}$ within each transmission phase. The *average service latency* for a node belonging to the $n^{\rm th}$ QoS-class is given by

$$\bar{t}_{{\rm s}n} = \mathbb{E}\{\mathsf{t}_{{\rm s}n}\} = \sum_{i=1}^{N_{\rm p}} \frac{\pi_n^{[i]}}{1 - x_n^{[0]}} \frac{1}{p_{\rm a}\boldsymbol{D}^{[i,n]}} \tag{24}$$

where $\pi_n^{[i]}/(1 - x_n^{[0]})$ represents the average time spent in the physical phase i. It is worth noting that the average waiting time in the buffer for unstable queues is infinite, while the average service latency is always finite according to (24).

The network percentile that achieves a target KPI value, e.g., total latency constrained to $t^\star$, is given by

$$\gamma_{\rm to} = \frac{1}{N}\sum_{n=1}^{N} \mathbb{1}_{\mathcal{T}}(n) \tag{25}$$

[14] Due to the ergodicity of the PPP, the notion of the network γ-stability coincides with the typical queue ϵ-stability defined in [29].

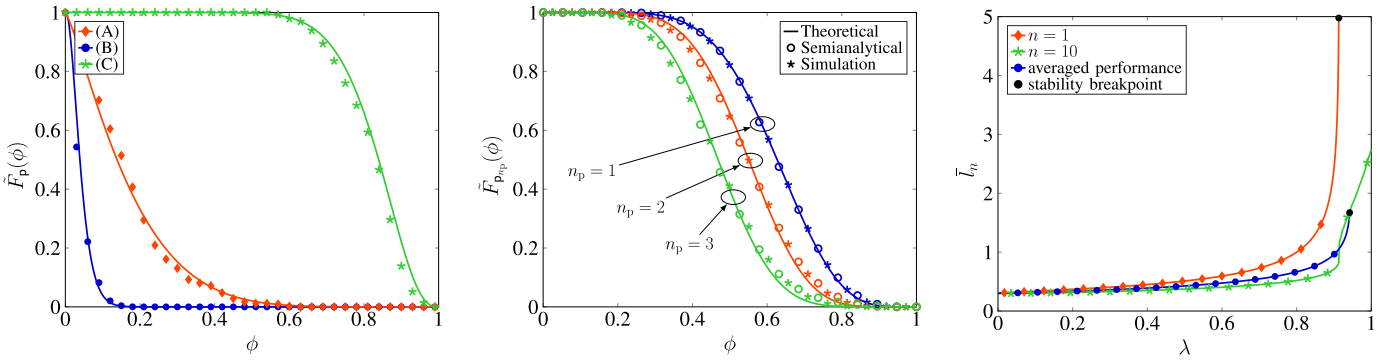

(a) Simple ALOHA. (b) Power-ramping ALOHA. (c) F-ALOHA.

Fig. 6. (a) CCDF of the TSP for $\mathcal{P}=\{-30\}$ [dBm]; (A): $\lambda=1.0$, $p_{\mathrm{a}}=0.2$, and $\theta=-30$ [dB]; (B): $\lambda=0.1$, $p_{\mathrm{a}}=0.6$, and $\theta=-23$ [dB]; (C): $\lambda=0.1$, $p_{\mathrm{a}}=0.2$, and $\theta=-30$ [dB]. (b) CCDF of the TSP for $\lambda=0.2$, $N_{\mathrm{c}}=1$, $N_{\mathrm{p}}=3$, $N_{\mathrm{t}}=1$, $\mathcal{P}=\{-30,-32,-34\}$ [dBm] (ramping-down), $p_{\mathrm{a}}=0.2$, and $\theta=-30$ [dB]. (c) Mean number of packets in the system as a function of node density for $N_{\mathrm{c}}=4$, $N_{\mathrm{p}}=1$, $\mathcal{P}=\{-30\}$ [dBm], $p_{\mathrm{a}}=0.4$, $\theta=-30$ [dB]. For all the subfigures we used: $N=10$, $\eta=2$, $R=10$ [m], $\sigma^2=-90$ [dBm], $a=0.1$ [packets/slots].

where $\mathcal{T}=\{n':\bar{t}_{n'}\leq t^{\star}\}$. Analogously to (21), we define the γ-*operativity region* by the function $\gamma_{\mathrm{to}}:\mathcal{G}\rightarrow[0,1]$ as

$$\mathcal{R}^{\mathrm{o}}_{\gamma}\triangleq\{\mathcal{R}:\gamma_{\mathrm{to}}(\mathcal{R})>\gamma\} \tag{26}$$

which determines the region of the points in the space of network parameters that satisfies a target performance (e.g., constrained total latency, queue length, etc.). In contrast to γ_{su}, that is more suited for *best-effort* type of traffic, γ_{to} is a metric more suited for *latency-sensitive* type of traffic.

VI. Numerical Results

We start by validating the developed spatiotemporal model, particularly Approximations 1-3, via the Monte Carlo simulations described in the sequel.

A. Monte Carlo Simulation Setting

The simulations are conducted over an arbitrary, yet fixed, realization of the PBN with wrapped-around boundaries.[15] Simulations are performed over a squared area of 9×10^5 $[\mathrm{m}^2]$, which is sufficient to have ergodicity with the considered node intensities $\lambda=\{0.1,0.2\}$ $[\mathrm{nodes}/\mathrm{m}^2]$ such that the realized network is considered as *typical*. Only the fading realizations and node activities change over the temporal domain. Each simulation run represents a time slot where independent channel gains are instantiated, packets are generated, and node interactions are established according to their protocol states and relative positions. The queue level, transmission power, and retransmission phase of each queue are tracked. For a transition from one time slot to another, packets are independently generated in all buffers with probability a. A transmitter with a non-empty buffer becomes active with probability p_{a} and uniformly selects one of the N_{c} channels. The SINRs at the receivers of all active links are determined based on the interferers that are simultaneously active on the same channel. Then, one packet is subtracted only from queues of the links with SINR greater than θ. The simulation starts with all idle nodes and runs for a sufficiently high number of time slots until the steady-state is reached. Let $\widehat{\boldsymbol{w}}^{[k]}$ be the estimated distribution of the physical phases at the k^{th} simulation run, then the steady-state is reached when $\max\|\widehat{\boldsymbol{w}}^{[k]}-\widehat{\boldsymbol{w}}^{[k-1]}\|<\epsilon$ where ϵ is a sufficiently small threshold (stop condition). The time slot at which the steady-state is reached is the time of the simulation kernel from which all temporal statistics are computed. We use $\epsilon=10^{-3}$ and a kernel of 10,000 iterations. The SINRs of the receivers of all active links along with the transmission powers of their intended transmitters are recorded to construct the meta distribution of SINRs for all power levels.

[15]The wrap-around simulation model is utilized to eliminate favorable interference conditions induced by network edges and their effects on queueing departure probabilities.

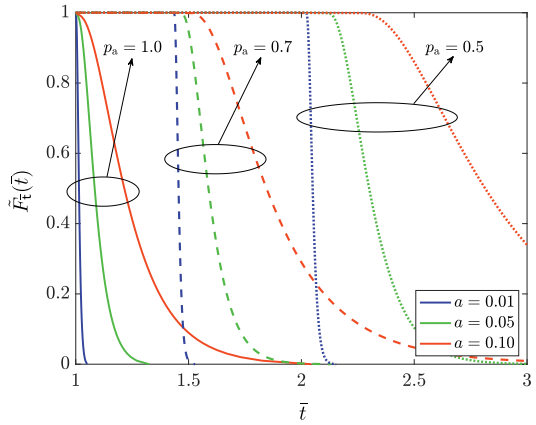

Fig. 7. CCDF of the mean total latency $\bar{\mathrm{t}}$ across the network for simple ALOHA with $\lambda=0.1$, $\theta=-30$ [dB], $R=10$ [m], and $a=0.1$.

B. Validation of the Framework

Figs. 6(a) and 6(b) show the CCDF of the TSP for different nodes intensities, ALOHA access probabilities, and transmission rates. In particular, Fig. 6(a) is plotted for a single power level ALOHA protocol and Fig. 6(b) is plotted for a power-ramping ALOHA protocol with three power levels. In both figures, the theoretical curves are plotted using (2) and the moments are obtained from Algorithm 2 after convergence. Both figures show a good agreement between the theoretical (solid lines) and simulation (markers) results, where $N=10$ QoS-classes are considered for the theoretical analysis. In particular, the Monte Carlo simulations with a fixed realization of the PBN account for the spatially correlated node activities and transmission powers (relaxed in Approximation 1), the exact fine-grained location-dependent performance (relaxed in Approximation 2), and the per-node temporally correlated transmission success (relaxed in Approximation 3). In addition to validating the developed mathematical framework, the figures also show the importance of the system parameters (i.e., node intensity, access probability, and transmission rates) on the distribution of the TSP.

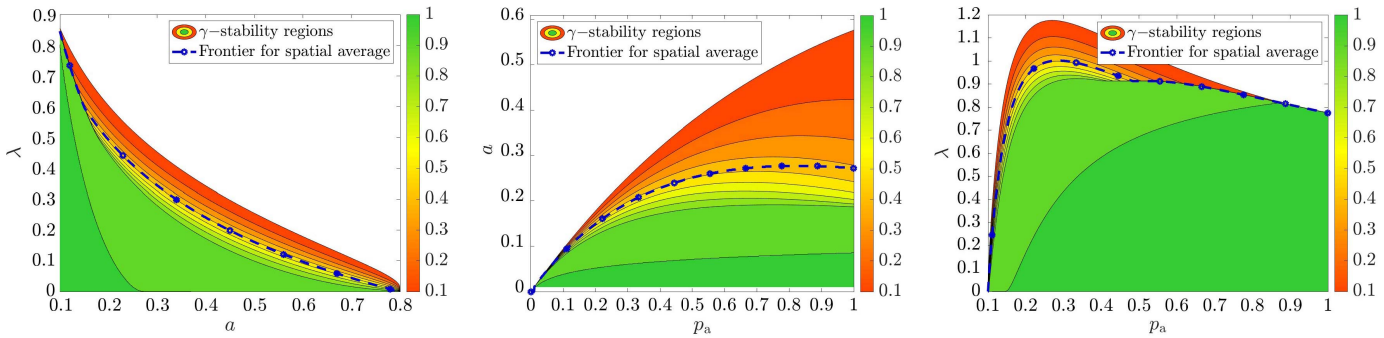

(a) (λ, a)-plane. (b) (p_a, a)-plane. (c) (p_a, λ)-plane.

Fig. 8. Stability regions of F-ALOHA over three different parameter planes. We show the γ-stablity regions for $N = 10$ (colorplot) and the deterministic stability frontier for the average performance (marked dashed curve). Where it is not differently stated $\lambda = 0.1$ $[\text{nodes/m}^2]$, $N_c = 4$, $\eta = 2$, $R = 10$ [m], $\theta = -30$ [dB], $\sigma^2 = -90$ [dBm], $\mathcal{P} = \{-30\}$ [dBm], $a = 0.1$ [packets/slots], and $p_a = 0.8$ [attempts/slots].

C. Performance Evaluation

Fig. 6(c) shows the average number of packets in the system as a function of the node density for the first ($n = 1$, red diamonds) and last ($n = 10$, green stars) QoS-classes with $N = 10$. The case of $N = 1$ (i.e., one queueing model for all the network with departure rate $p_a M_1$) is also considered. Although an infinite queue size is considered in the analysis, the figure shows that a finite queue with reasonable buffer size is required as long as the node operates within a stable QoS-class. If the queue is unstable, the packets will overflow with probability one regardless of the buffer size. Note that the curve of the highest class (i.e., $N = 10$) experiences a change of slope at the point where a lower class becomes unstable. Such variation occurs because all nodes within the unstable class (i.e., $1/N$ fraction of the total nodes) become always active, thus increasing the interference.

Fig. 7 shows the CCDF of the mean total latency across the network, which is obtained by the per-class characterization through (23a) with a sufficient number (i.e. $N = 100$) of classes. Due to the ALOHA transmission deferrals, the channel access probability p_a determines the minimum packet latency. Transmitted packets are susceptible to larger latencies due to channel variations and interference, which leads to transmission failures. However, as the traffic becomes lighter (i.e., low a), the interference is relieved and p_a becomes the limiting factor for the latency.

Fig. 8 shows the Pareto frontier for the system parameters that ensures queuing stability for a fraction γ of the nodes. Each colored region shows the pairs of network parameters that are required to ensure stability for a given fraction of nodes. The blue dashed line with markers, denoted as *stability frontier for spatially averaged performance*, shows the region of the network parameters leading to a spatially averaged departure rate greater than the packet generation rate,[16] i.e.,

$$\mathcal{R}^{s}_{av} \triangleq \{\mathcal{R} : p_a M_1(\mathcal{R}) > a\} \tag{27}$$

where we have considered the function $M_1 : \mathcal{G} \rightarrow [0, 1]$. Such classical approach does not convey any information on the fraction of nodes that have unstable queue. On the contrary, our approach based on the meta distribution reveals the percentile of stable and unstable nodes. The results shown in Fig. 8 are of primary importance to characterize the scalability vs. stability tradeoff for *best-effort*[17] traffic in MWNs. In particular, the maximum spatial traffic density of nodes that can be accommodated subject to a γ-stability constraint is shown by considering F-ALOHA with $N_c = 4$. In particular, Fig. 8(a) shows the (λ, a)-pairs that F-ALOHA can accommodate subject to a given γ-stability constraint with $p_a = 0.8$. To accommodate more nodes may necessitate a lower traffic generation to maintain the same γ-percentile of stable nodes. Fig. 8 also shows the importance of choosing the proper value for the access probability p_a of the F-ALOHA to ensure a stable network operation. Fig. 8(b) shows the regions on the (p_a, a)-plane where γ-stability holds for $\lambda = 0.1$ [node/m^2]. It can be observed that p_a must be greater than a to allow any fraction of the network to be stable, since a sufficiently persistent channel access is a necessary but not sufficient condition for stability. Note that, for a given γ and increasing a, the minimum p_a ensuring γ-stability diverges increasingly from $p_a = a$. Fig. 8(c) shows the Pareto frontiers for regions of the (p_a, λ)-pairs. It can be observed that there is a given range of p_a values that ensures stability for a given λ. This is because the tradeoff between conservative and aggressive channel access should be balanced to maintain stable queues. Employing a conservative access policy with low values of p_a misses many transmission opportunities, accumulates packets in buffers, and leads to instability. On the other hand, employing an aggressive access policy with high values of p_a aggravates the interference, leads to excessive transmission failures due to low SINR, thus leading to instability.

Fig. 9 shows the Pareto frontiers, as well as the NC and SC frontiers, for different operational objectives of the considered uncoordinated MWNs. Particularly, Fig. 9 considers the uncoordinated MWN operation with (a) γ-stability for $\gamma = 0.99$ constraint, (b) γ-operativity for a latency $t^\star \leq 5$ [slots] and $\gamma = 0.5$, and (c) γ-operativity for a latency $t^\star \leq 3$ [slots] and $\gamma = 0.05$. Note that the frontiers obtained by considering dominant systems, i.e., NC and SC conditions, do not respectively provide tight upper and lower bounds of the actual performance. This may either lead to an over conservative transmission protocol with a consistent waste of resources or to an over aggressive one that violates the KPI constraints. In particular, designing the network according to the SC constraints may lead to serving a much lower intensity of nodes that the network can support. On the other hand,

[16] For simplicity, in the case of (27) we show the condition for single phase, i.e., Geo/Geo/1 queues.

[17] Best-effort traffic is tolerant to latency and, therefore, a finite latency is the main requirement.

TABLE I
UMA STRATEGY DESIGN

	N_{p}	N_{t}	$\mathcal{P}$ [dBm]	γ_{su}	γ_{to} $(t^\star = 5)$	γ_{to} $(t^\star = 10)$	$w^{[0]}$
Single power	1	1	$\{-30\}$	0.4	0.1	0.4	0.15
Ramping-down 1	4	1	$\{-30, -32, -34, -40\}$	0.4	0	0.2	0.10
Ramping-down 2	4	10	$\{-30, -32, -34, -40\}$	0.6	0.2	0.5	0.25
Ramping-up 1	4	1	$\{-30, -28, -26, -22\}$	0.3	0	0.2	0.09
Ramping-up 2	4	10	$\{-30, -28, -26, -22\}$	0.2	0	0.2	0.06

designing the network according to the NC may result in serving a lot more nodes than the network should support and violating the constraints on KPI values. Hence, Fig. 9 manifests the importance of the developed spatiotemporal model to determine the network scalability under the required network operational constraints.

D. Network Design

To show the impact of the power-ramping strategy, we present a network design with $\lambda = 0.1$, $\theta = -23$ [dB], $\sigma^2 = -90$ [dBm], $a = 0.1$, $\eta = 2$, $R = 10$ [m] and $N = 10$. The considered setting is in accordance with LoRa dense ad-hoc scenario (i.e., $\lambda = 0.1$ [nodes/m^2]) for low-power consumption and short-range communications. Table I presents four different design of UMA strategies in terms of number of powers, power-ramping scheme, and persistence: (i) Single power, (ii) Ramping-down 1, (iii) Ramping-down 2, (iv) Ramping-up 1, and (v) Ramping-up 2. Table I also shows the performance corresponding to each scheme in terms of the fraction γ_{su} of stable nodes, the fraction γ_{to} of nodes with latency less than $t^\star$ time slots, and the spatially averaged probability of empty buffer $w^{[0]}$. The results in the table emphasize that ramping-down power control with some persistence (i.e., Ramping-down 1) outperforms all other schemes.[18] This is because ramping-down the power relieves the interference and the persistence on each power level ensures sacrificing the performance of nodes belonging to low QoS-classes. Ramping-down without persistence may mistakenly degrade the performance of nodes belonging to high QoS-classes that experience instantaneous severe fading conditions. The table also shows that ramping-up the power has the worst performance among all schemes, which is because ramping-up the power aggravates the interference without enhancing the performance of nodes at congested locations. Moreover, the single-power ALOHA scheme outperforms a ramping-down scheme when it is not properly designed.

Remark 5: The employed power ramping scheme is simple and distributed. Each device locally determines its power level from its buffer state and its previous transmission experience. Nevertheless, the number of power levels N_{p}, persistence per level N_{t}, ramping strategy (i.e., up or down), and power level values in $\mathcal{P}$ are determined offline taking into account the global network performance along with the application QoS requirements (see, e.g., Fig. 8). This leads to a context-aware design and low-complexity operation.

VII. FINAL REMARK

This paper combines stochastic geometry and queueing theory to develop a spatiotemporal model for design and analysis of uncoordinated MWN. Macroscopic- and microscopic-scale analyses are carried out through an iterative procedure that tracks the number of packets in the transmitter buffers, channel access, transmission power, and the retransmission phase. The developed framework accounts for the location-dependent performance and interference temporal correlation via the meta distribution of the SINR. In particular, the network is partitioned into N equiprobable QoS-classes, where the performance of a given QoS-class is explicitly determined and the percentile performance of the network is characterized. To this end, the concepts of γ-stability and γ-operativity are introduced, respectively, to characterize the percentile of the network with stable nodes and that with desired performance.

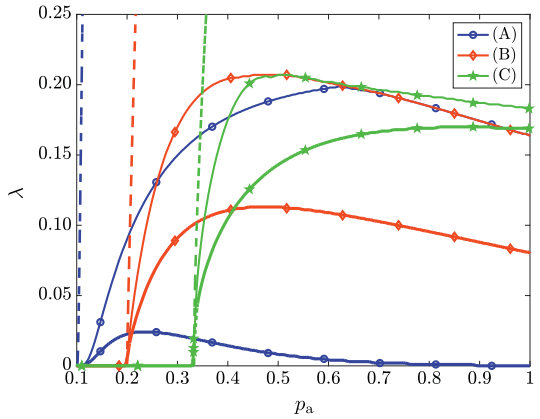

Fig. 9. Pareto frontiers for the necessary (dashed), sufficient (dotted), and actual (solid) conditions for ALOHA for (A): γ-stability, with $a = 0.1$ and $\gamma = 0.999$; (B): γ-operativity, with $t^\star = 5$ [slots] and $\gamma = 0.5$; and (C): with $t^\star = 3$ [slots] and $\gamma = 0.05$. Other variables are as in Fig. 8.

The tradeoff between scalability, stability, and other KPIs is shown via the Pareto frontiers of the γ-stability and γ-operativity regions, by accounting for the per-node traffic intensity, node density, target transmission rate, and uncoordinated access persistence. The analysis accounting only for dominant systems is inadequate and it is shown that location-dependent queueing states must be accounted for designing the network. To this end, the developed framework is also used to design UMA with different power-ramping schemes. The importance of power-ramping design is manifested through a case study that reveals the superiority of the ramping-down scheme over the ramping-up scheme when considering the network performance. The results also manifest the importance of power level persistence to mitigate the effect of fading on the power control and the dominance of the access probability on the minimum achievable latency. This work quantifies the scalability of UMA in MWNs, unleashes a traffic-aware network design, and paves the way to new applications for IoT and CPSs.

[18]Note that a similar insight was proved in [48] for uplink in cellular networks where nodes have saturated buffers.

APPENDIX
PROOF OF THEOREM 1

The TSP at the typical point of Π is given by

$$\mathsf{p}_{n_\mathrm{p}} \triangleq \mathbb{P}\{\mathsf{z}_\circ > \theta|\Pi\} = \mathbb{P}\Big\{\frac{P_{n_\mathrm{p}}\mathsf{h}_\circ R^{-2\eta}}{(\mathsf{i}_\circ+\sigma^2)} > \theta|\Pi\Big\} \quad (28a)$$

$$= e^{-\theta_{n_\mathrm{p}}\sigma^2} \prod_{j\,:\,\mathbf{y}_j\in\Pi\setminus\mathbf{y}_\circ} \Big(\sum_{i=1}^{N_\mathrm{p}} \frac{p_\mathrm{fa}w^{[i]}}{1+\theta_{n_\mathrm{p},i}\|\mathbf{y}_j\|^{-2\eta}} + 1 - p_\mathrm{fa}\sum_{i=1}^{N_\mathrm{p}} w^{[i]}\Big) \quad (28b)$$

with $\mathsf{i}_\circ = \sum_{j\,:\,\mathbf{y}_j\in\Pi\setminus\mathbf{y}_\circ} \mathsf{p}_j\mathsf{a}_j\mathsf{h}_j\|\boldsymbol{y}_j\|^{-2\eta}$,[19] $\theta_{n_\mathrm{p}} = \theta R^{2\eta}/P_{n_\mathrm{p}}$, and $\theta_{n_\mathrm{p},i} = \theta_{n_\mathrm{p}}P_i$. The (28b) follows from (i) the exponential distribution of the channel gain, (ii) the averaging over the F-ALOHA, (iii) the averaging over the physical-phase distribution (by Approximation 1), and (iv) the averaging over channel gains.[20] Hence the b^{th}-order statistical moment is found to be

$$M_{b,n_\mathrm{p}} \triangleq \mathbb{E}^\circ\{\mathsf{p}_{n_\mathrm{p}}^b\} = e^{-b\theta_{n_\mathrm{p}}\sigma^2}\exp\Big\{-\lambda\frac{\pi}{\eta}\sum_{k=1}^{b}\binom{b}{k}(-1)^{k+1} \times \int_0^\infty \Big(-\sum_{i=1}^{N_\mathrm{p}} p_\mathrm{fa}\frac{w^{[i]}\theta_{n_\mathrm{p},i}}{u+\theta_{n_\mathrm{p},i}}\Big)^k u^{\frac{1-\eta}{\eta}}\,du\Big\} \quad (29)$$

that follows from the probability generating functional (PGFL) of the PPP, with $(1+v)^b = \sum_{k=0}^{b}\binom{b}{k}v^k$, by rearranging the terms, transforming to polar coordinates, and changing the integration variable to $u \triangleq \|\boldsymbol{y}_j\|^{2\eta}$. Finally, equations (5) and (6) readily follow as distinct special cases of (29) for (i) $b=1$ with generic N_p and (ii) $b=1,2$ with $N_\mathrm{p}=1$, respectively.

REFERENCES

[1] A. Al-Fuqaha, M. Guizani, M. Mohammadi, M. Aledhari, and M. Ayyash, "Internet of things: A survey on enabling technologies, protocols, and applications," *IEEE Commun. Surveys Tuts.*, vol. 17, no. 4, pp. 2347–2376, 4th Quart., 2015.

[2] D. S. Nunes, P. Zhang, and J. S. Silva, "A survey on human-in-the-loop applications towards an Internet of all," *IEEE Commun. Surveys Tuts.*, vol. 17, no. 2, pp. 944–965, 2nd Quart., 2015.

[3] A. Laya, C. Kalalas, F. Vazquez-Gallego, L. Alonso, and J. Alonso-Zarate, "Goodbye, ALOHA!" *IEEE Access*, vol. 4, pp. 2029–2044, 2016.

[4] A. Bader, H. ElSawy, M. Gharbieh, M.-S. Alouini, A. Adinoyi, and F. Alshaalan, "First mile challenges for large-scale IoT," *IEEE Commun. Mag.*, vol. 55, no. 3, pp. 138–144, Mar. 2017.

[5] M. S. Ali, E. Hossain, and D. I. Kim, "LTE/LTE-A random access for massive machine-type communications in smart cities," *IEEE Commun. Mag.*, vol. 55, no. 1, pp. 76–83, Jan. 2017.

[6] L. Vangelista, A. Zanella, and M. Zorzi, "Long-range IoT technologies: The dawn of LoRa^{TM}" in *Proc. Future Access Enablers Ubiquitous Intell. Infrastruct.* New York, NY, USA: Springer, 2015, pp. 51–58.

[7] Y.-P. E. Wang *et al.*, "A primer on 3GPP narrowband Internet of Things," *IEEE Commun. Mag.*, vol. 55, no. 3, pp. 117–123, Mar. 2017.

[8] F. Meyer, B. Etzlinger, Z. Liu, F. Hlawatsch, and M. Z. Win, "A scalable algorithm for network localization and synchronization," *IEEE Internet Things J.*, vol. 5, no. 6, pp. 4714–4727, Dec. 2018.

[9] Y. Xiong, N. Wu, Y. Shen, and M. Z. Win, "Cooperative network synchronization: Asymptotic analysis," *IEEE Trans. Signal Process.*, vol. 66, no. 3, pp. 757–772, Feb. 2018.

[10] R. R. Rao and A. Ephremides, "On the stability of interacting queues in a multiple-access system," *IEEE Trans. Inf. Theory*, vol. 34, no. 5, pp. 918–930, Sep. 1988.

[11] V. Anantharam, "The stability region of the finite-user slotted ALOHA protocol," *IEEE Trans. Inf. Theory*, vol. 37, no. 3, pp. 535–540, May 1991.

[19]The receiver of the typical link is considered at the origin without any loss of generality.

[20]For the averaging over channels we utilize the Laplace transform of the exponential PDF of the channel gain [25].

[12] W. Luo and A. Ephremides, "Stability of N interacting queues in random-access systems," *IEEE Trans. Inf. Theory*, vol. 45, no. 5, pp. 1579–1587, Jul. 1999.

[13] A. Ephremides and R.-Z. Zhu, "Delay analysis of interacting queues with an approximate model," *IEEE Trans. Commun.*, vol. COM-35, no. 2, pp. 194–201, Feb. 1987.

[14] L. Tassiulas and A. Ephremides, "Dynamic server allocation to parallel queues with randomly varying connectivity," *IEEE Trans. Inf. Theory*, vol. 39, no. 2, pp. 466–478, Mar. 1993.

[15] M. J. Neely, "Order optimal delay for opportunistic scheduling in multi-user wireless uplinks and downlinks," *IEEE/ACM Trans. Netw.*, vol. 16, no. 5, pp. 1188–1199, Oct. 2008.

[16] N. Pappas, M. Kountouris, and A. Ephremides, "The stability region of the two-user interference channel," in *Proc. IEEE Inf. Theory Workshop*, Sep. 2013, pp. 1–5.

[17] N. Pappas and M. Kountouris, "The stability region of the two-user broadcast channel," in *Proc. IEEE Int. Conf. Commun.*, no. 5, May 2016, pp. 1–6.

[18] G. D. Çelik and E. Modiano, "Scheduling in networks with time-varying channels and reconfiguration delay," *IEEE/ACM Trans. Netw.*, vol. 23, no. 1, pp. 99–113, Feb. 2015.

[19] M. J. Neely, E. Modiano, and C. E. Rohrs, "Dynamic power allocation and routing for time-varying wireless networks," *IEEE J. Sel. Areas Commun.*, vol. 23, no. 1, pp. 89–103, Jan. 2005.

[20] M. Z. Win, P. C. Pinto, A. Giorgetti, M. Chiani, and L. A. Shepp, "Error performance of ultrawideband systems in a Poisson field of narrowband interferers," in *Proc. IEEE 9th Int. Symp. Spread Spectr. Techn. Appl.*, Manaus, Brazil, Aug. 2006, pp. 410–416.

[21] M. Z. Win, P. C. Pinto, and L. A. Shepp, "A mathematical theory of network interference and its applications," *Proc. IEEE*, vol. 97, no. 2, pp. 205–230, Feb. 2009.

[22] M. Haenggi, J. G. Andrews, F. Baccelli, O. Dousse, and M. Franceschetti, "Stochastic geometry and random graphs for the analysis and design of wireless networks," *IEEE J. Sel. Areas Commun.*, vol. 27, no. 7, pp. 1029–1046, Sep. 2009.

[23] P. C. Pinto and M. Z. Win, "Communication in a poisson field of interferers—Part I: Interference distribution and error probability," *IEEE Trans. Wireless Commun.*, vol. 9, no. 7, pp. 2176–2186, Jul. 2010.

[24] P. C. Pinto and Moe Z. Win, "Communication in a poisson field of interferers—Part II: Channel capacity and interference spectrum," *IEEE Trans. Wireless Commun.*, vol. 9, no. 7, pp. 2187–2195, Jul. 2010.

[25] H. ElSawy, A. Sultan-Salem, M. S. Alouini, and M. Z. Win, "Modeling and analysis of cellular networks using stochastic geometry: A tutorial," *IEEE Commun. Surveys Tuts.*, vol. 19, no. 1, pp. 167–203, 1st Quart., 2017.

[26] K. Stamatiou and M. Haenggi, "Random-access poisson networks: Stability and delay," *IEEE Commun. Lett.*, vol. 14, no. 11, pp. 1035–1037, Nov. 2010.

[27] P. H. J. Nardelli, M. Kountouris, P. Cardieri, and M. Latva-aho, "Throughput optimization in wireless networks under stability and packet loss constraints," *IEEE Trans. Mobile Comput.*, vol. 13, no. 8, pp. 1883–1895, Aug. 2014.

[28] Y. Zhou and W. Zhuang, "Performance analysis of cooperative communication in decentralized wireless networks with unsaturated traffic," *IEEE Trans. Wireless Commun.*, vol. 15, no. 5, pp. 3518–3530, May 2016.

[29] Y. Zhong, M. Haenggi, T. Q. S. Quek, and W. Zhang, "On the stability of static poisson networks under random access," *IEEE Trans. Commun.*, vol. 64, no. 7, pp. 2985–2998, Jul. 2016.

[30] M. Gharbieh, H. ElSawy, A. Bader, and M.-S. Alouini, "Spatiotemporal stochastic modeling of IoT enabled cellular networks: Scalability and stability analysis," *IEEE Trans. Commun.*, vol. 65, no. 8, pp. 3585–3600, Aug. 2017.

[31] Y. Zhong, T. Q. S. Quek, and X. Ge, "Heterogeneous cellular networks with spatio-temporal traffic: Delay analysis and scheduling," *IEEE J. Sel. Areas Commun.*, vol. 35, no. 6, pp. 1373–1386, Jun. 2017.

[32] G. Chisci, H. ElSawy, A. Conti, M.-S. Alouini, and M. Z. Win, "On the scalability of uncoordinated multiple access for the Internet of things," in *Proc. Int. Symp. Wireless Commun. Syst.*, Bologna, Italy, Aug. 2017, pp. 402–407.

[33] M. Kountouris, N. Pappas, and A. Avranas, "QoS provisioning in large wireless networks," in *Proc. Int. Symp. Modeling Optim. Mobile, Ad Hoc, Wireless Netw. (WiOpt)*, May 2018, pp. 1–6.

[34] M. Kaynia, N. Jindal, and G. E. Oien, "Improving the performance of wireless ad hoc networks through MAC layer design," *IEEE Trans. Wireless Commun.*, vol. 10, no. 1, pp. 240–252, Jan. 2011.

[35] B. Blaszczyszyn and P. Muhlethaler, "Stochastic analysis of non-slotted aloha in wireless ad-hoc networks," in *Proc. IEEE Conf. Comput. Commun. (INFOCOM)*, Mar. 2010, pp. 1–9.

[36] A. Munari, P. Mähönen, and M. Petrova, "A stochastic geometry approach to asynchronous ALOHA full-duplex networks," *IEEE/ACM Trans. Netw.*, vol. 25, no. 6, pp. 3695–3708, Dec. 2017.
[37] M. Haenggi, "The meta distribution of the SIR in Poisson bipolar and cellular networks," *IEEE Trans. Wireless Commun.*, vol. 15, no. 4, pp. 2577–2589, Apr. 2016.
[38] M. Salehi, A. Mohammadi, and M. Haenggi, "Analysis of D2D underlaid cellular networks: SIR meta distribution and mean local delay," *IEEE Trans. Commun.*, vol. 65, no. 7, pp. 2904–2916, Jul. 2017
[39] Y. Wang, M. Haenggi, and Z. Tan, "The meta distribution of the SIR for cellular networks with power control," *IEEE Trans. Commun.*, vol. 66, no. 4, pp. 1745–1757, Apr. 2018.
[40] H. ElSawy and M.-S. Alouini, "On the meta distribution of coverage probability in uplink cellular networks," *IEEE Commun. Lett.*, vol. 21, no. 7, pp. 1625–1628, Jul. 2017.
[41] M. Haenggi, *Stochastic Geometry for Wireless Networks*. Cambridge, U.K.: Cambridge Univ. Press, 2013.
[42] V. Chandrasekhar and J. G. Andrews, "Spectrum allocation in tiered cellular networks," *IEEE Trans. Commun.*, vol. 57, no. 10, pp. 3059–3068, Oct. 2009.
[43] S. Graf and H. Luschgy, *Foundations of Quantization for Probability Distributions* (Lecture Notes in Mathematics), 1st ed. Berlin, Germany: Springer-Verlag, 2000.
[44] A. S. Alfa, *Applied Discrete-Time Queues*, 2nd ed. New York, NY, USA: Springer, 2016.
[45] R. M. Loynes, "The stability of a queue with non-independent inter-arrival and service times," *Math. Proc. Cambridge Philos. Soc.*, vol. 58, no. 5, pp. 497–520, 1962.
[46] D. P. Bertsekas and R. G. Gallager, *Data Networks*, 2nd ed. Upper Saddle River, NJ, USA: Prentice-Hall, 1992.
[47] L. Kleinrock, *Queuing Systems: Theory*, 1st ed. Hoboken, NJ, USA: Wiley, 1975.
[48] R. Arshad, L. H. Afify, Z. Liu, H. ElSawy, T. Y. Al-Naffouri, and M.-S. Alouini, "On the effect of uplink power control on temporal retransmission diversity," *IEEE Wireless Commun. Lett.*, vol. 8, no. 1, pp. 309–312, Feb. 2019.

Giovanni Chisci (S'15–M'18) received the Laurea degree *(summa cum laude)* in electrical engineering from the University of Florence, Italy, in 2014, and the Ph.D. degree in information engineering from the University of Ferrara, Italy, in 2018, where he is currently enrolled as a Postdoctoral Fellow.

He was with the Wireless Information and Network Sciences Laboratory at the Massachusetts Institute of Technology, and with the Computer, Electrical and Mathematical Sciences and Engineering Division at the King Abdullah University of Science and Technology in 2016 and 2018, respectively. His research encompasses fundamental theories and algorithm design for wireless networks and complex systems. His current research topics include intrinsic network secrecy, low latency networks, and cyber physical systems. He served as a TPC member for IEEE conferences and as a reviewer for IEEE journals.

Hesham ElSawy (S'10–M'14–SM'17) received the Ph.D. degree in electrical engineering from the University of Manitoba, Canada, in 2014. He joined the Electrical Engineering Department, King Fahd University of Petroleum and Minerals, Saudi Arabia, as an Assistant Professor in Fall 2018. Prior to that, he was a Post-Doctoral Fellow at the King Abdullah University of Science and Technology, Saudi Arabia, a Research Assistant at TRTech, Winnipeg, MB, Canada, and a Telecommunication Engineer at the National Telecommunication Institute, Egypt. His research interests include statistical modeling of wireless networks, stochastic geometry, and queueing analysis for wireless communication networks. He received several academic awards including the NSERC Industrial Postgraduate Scholarship from 2010 to 2013, and the TRTech Graduate Students Fellowship from 2010 to 2014. He coauthored three award-winning papers that are recognized by the IEEE COMSOC Best Survey Paper Award, the Best Scientific Contribution Award to the IEEE International Symposium on Wireless Communication Systems 2017, and the Best Paper Award in Small Cell and 5G Networks (SmallNets) Workshop of the 2015 IEEE International Conference on Communications. He is recognized as an Exemplary Reviewer by the IEEE TRANSACTIONS ON COMMUNICATIONS for the three concessive years (2014–2016), and by the IEEE TRANSACTIONS ON WIRELESS COMMUNICATIONS in 2017.

Andrea Conti (S'99–M'01–SM'11) received the Laurea *(summa cum laude)* in telecommunications engineering and the Ph.D. in electronic engineering and computer science from the University of Bologna, Italy, in 1997 and 2001, respectively.

He is a Professor at the University of Ferrara, Italy. Prior to joining the University of Ferrara, he was with the Consorzio Nazionale Interuniversitario per le Telecomunicazioni and with the IEIIT-Consiglio Nazionale delle Ricerche. In Summer 2001, he was with the Wireless Systems Research Department at AT&T Research Laboratories. Since 2003, he has been a frequent visitor to the Wireless Information and Network Sciences Laboratory at the Massachusetts Institute of Technology, where he presently holds the Research Affiliate appointment. His research interests involve theory and experimentation of wireless systems and networks including network localization, distributed sensing, adaptive diversity communications, and network secrecy. He is recipient of the HTE Puskás Tivadar Medal and co-recipient of the IEEE Communications Society's Stephen O. Rice Prize in the field of Communications Theory and of the IEEE Communications Society's Fred W. Ellersick Prize.

Dr. Conti has served as editor for IEEE journals, as well as chaired international conferences. He has been elected Chair of the IEEE Communications Society's Radio Communications Technical Committee. He is a co-founder and elected Secretary of the IEEE Quantum Communications & Information Technology Emerging Technical Subcommittee. He is an elected Fellow of the IET and has been selected as an IEEE Distinguished Lecturer.

Mohamed-Slim Alouini (S'94–M'98–SM'03–F'09) was born in Tunis, Tunisia. He received the Ph.D. degree in electrical engineering from the California Institute of Technology (Caltech), Pasadena, CA, USA, in 1998. He served as a Faculty Member at the University of Minnesota, Minneapolis, MN, USA, and then at the Texas A&M University at Qatar, Education City, Doha, Qatar, before joining the King Abdullah University of Science and Technology, Thuwal, Makkah province, Saudi Arabia, as a Professor of electrical engineering in 2009. His current research interests include the modeling, design, and performance analysis of wireless communication systems.

Moe Z. Win (S'85–M'87–SM'97–F'04) is a Professor at the Massachusetts Institute of Technology (MIT) and the founding director of the Wireless Information and Network Sciences Laboratory. Prior to joining MIT, he was with AT&T Research Laboratories and NASA Jet Propulsion Laboratory.

His research encompasses fundamental theories, algorithm design, and network experimentation for a broad range of real-world problems. His current research topics include network localization and navigation, network interference exploitation, and quantum information science. He has served the IEEE Communications Society as an elected Member-at-Large on the Board of Governors, as elected Chair of the Radio Communications Committee, and as an IEEE Distinguished Lecturer. Over the last two decades, he held various editorial positions for IEEE journals and organized numerous international conferences. Currently, he is serving on the SIAM Diversity Advisory Committee.

Dr. Win is an elected Fellow of the AAAS, the IEEE, and the IET. He was honoured with two IEEE Technical Field Awards: the IEEE Kiyo Tomiyasu Award (2011) and the IEEE Eric E. Sumner Award (2006, jointly with R. A. Scholtz). Together with students and colleagues, his papers have received several awards. Other recognitions include the IEEE Communications Society Edwin H. Armstrong Achievement Award (2016), the International Prize for Communications Cristoforo Colombo (2013), the Copernicus Fellowship (2011) and the *Laurea Honoris Causa* (2008) from the Universitá degli Studi di Ferrara, and the U.S. Presidential Early Career Award for Scientists and Engineers (2004). He is an ISI Highly Cited Researcher.